AN ABSTRACT OF THE THESIS OF

Victor Robert Corsiglia for the M. S. in Mechanical Engineering
(Name) (Degree) (Major)

Date thesis is presented March 27, 1963

Title A CALCULATION OF THE SUCTION REQUIREMENTS TO PREVENT BOUNDARY LAYER SEPARATION ON A CIRCULAR CYLINDER

Abstract approved [redacted]
(Major professor)

An investigation was made to test the method of Head on the flow about a circular cylinder with suction. The method of Head is an approximate method of obtaining solutions to the boundary layer equations. The method was adapted to the digital computer to facilitate performing the calculations, and a variety of suction distributions were studied. In the cases where an exact solution of the boundary layer equations was available the results were compared.

The method predicted a point of separation comparable to exact solutions for the case in which the suction velocity was zero. However, for the large suction velocities and large adverse pressure gradients associated with the circular cylinder, the method broke down. Enough information was obtained before breakdown to indicate that another approximate method due to Ando underestimates the suction required to prevent separation.

A CALCULATION OF THE SUCTION REQUIREMENTS TO PREVENT BOUNDARY LAYER SEPARATION ON A CIRCULAR CYLINDER

by

VICTOR ROBERT CORSIGLIA

A THESIS

submitted to

OREGON STATE UNIVERSITY

in partial fulfillment of
the requirements for the
degree of

MASTER OF SCIENCE

June 1963

APPROVED:

[redacted]

Assistant Professor of Mechanical and Industrial Engineering

In Charge of Major

[redacted]

Head of Department of Mechanical and Industrial Engineering

[redacted]

Dean of Graduate School

Date thesis is presented March 27, 1963

Typed by Jolene Wuest

ACKNOWLEDGMENT

I wish to express my appreciation to Mr. E. W. Geller for suggesting this thesis topic to me and for his invaluable assistance during the course of the investigation. I am grateful to the Research Council for the financial assistance in meeting the computing expenses.

TABLE OF CONTENTS

LIST OF FIGURES

LIST OF TABLES

LIST OF SYMBOLS

c	Diameter of circular cylinder (characteristic dimension)
x, y	Rectangular coordinates of position
δ	y at u=U (boundary layer thickness)
u, v	Rectangular components of velocity within the boundary layer
U_o	Free stream velocity
U	Velocity at edge of the boundary layer
v_s	Velocity at the surface in the direction of y negative
P	Pressure
$\overline{U}$	$\overline{U} = U/U_o$
η	$\eta = y/\delta$
$\overline{x}$	$\overline{x} = x/c$
v_s^*	$v_s^* = v_s/U_o\sqrt{U_o\, c/\nu}$
ϕ	Angular coordinate of position (see Figure 20)
ϕ_s	Stagnation value of angle ϕ (see Figure 20)
μ	Viscosity
ρ	Density
ν	$\nu = \mu/\rho$
t^*	$t^* = (\theta/c)^2\, U_o\, c/\nu$
ℓ	$\ell = (\theta/U)\ (\partial u/\partial y)_o$
m	$m = (\theta^2/U)\ (\partial^2 u/\partial y^2)_o$
θ	Momentum thickness (see Section IV.)
δ^*	Displacement thickness (see Section IV.)
ϵ	Energy thickness (see Section IV.)

D^* Dissipation integral (see Section IV.)

H $H = \delta^*/\theta$ shape factor

λ Pohlhausen parameter and also used as $\lambda = \sqrt{t^*}\, v_s^*$

Λ $\Lambda = t^* \overline{U}'$

A CALCULATION OF THE SUCTION REQUIREMENTS TO PREVENT BOUNDARY LAYER SEPARATION ON A CIRCULAR CYLINDER

I. INTRODUCTION

Problems in aerodynamics which are concerned with such phenomena as flow separation and drag involve the concept of the boundary layer for their analysis. In 1904 L. Prandtl presented a paper entitled, "Fluid Motion With Very Small Friction", to the Mathematical Congress in Heidelberg in which he sought to explain the existence of considerable drag on bodies in the flow of fluids of small viscosity. This paper showed that the flow of fluids could be divided into two regions, a thin layer near the surface on the body where viscous stresses are significant and the region outside of this thin layer where the fluid can be taken to be inviscid.

Prandtl observed that the velocity of the fluid passing over a solid body approached zero as the surface of the body was neared. This boundary condition gave rise to a velocity gradient in which the velocity changed from the zero value at the surface to the value given by a solution of the problem of an inviscid fluid flowing over the same body. He further showed that this velocity gradient was large, since the thickness of this region was small with respect to the dimensions of the body. This is the region referred to as the boundary layer.

The important implication of this concept of the boundary layer is that the fluid can be analyzed separately as two distinct regions, the boundary layer region in which viscous stresses are significant and the region outside of the boundary layer in which the viscous stresses can be neglected. This thesis is concerned with the happenings inside of the boundary layer, hence the effect of the outside flow is taken to be known, and this effect appears as a boundary condition of pressure and velocity at the outer edge of the boundary layer.

As a consequence of the presence of the boundary layer we are able to focus our attention on the thin layer near the surface of a body where the viscous stresses predominate. In general, to deal with the dynamics of a viscous fluid, the Navier-Stokes equations must be used which are the expression of Newton's second law for a fluid with viscous shearing stresses present. These Navier-Stokes equations have not been solved except for a few special cases. Fortunately their use with the concept of the boundary layer allows considerable simplification, and the simplified equations are called the boundary layer equations. Here again, a practical complication is encountered in that exact solutions are known for only several special cases, and given an arbitrary airfoil to study the chance of obtaining a solution is slight. Two exact solutions are mentioned in the next section.

A great variety of problems can be analyzed by using

approximate techniques involving the use of the momentum integral relation and the energy integral relation. One such technique, that of Pohlhausen, will be discussed later. Among the many techniques that have evolved from Pohlhausen's original work is that of Head, which is the method of this thesis.

II. BOUNDARY LAYER EQUATIONS

The presentation of equations will be begun with the boundary layer equations, and a knowledge on the part of the reader of their derivation from basic principles and the Navier-Stokes equations will be presumed. This derivation can be found in any of several references (11, p. 132-138).

The two basic equations of this thesis are the boundary layer equation written for two-dimensional incompressible flow

$$u\frac{\partial u}{\partial x} + v\frac{\partial u}{\partial y} = U\frac{dU}{dx} + \nu\frac{\partial^2 u}{\partial y^2} \tag{1}$$

and the equation of continuity

$$\frac{\partial u}{\partial x} + \frac{\partial v}{\partial y} = o \tag{2}$$

As was mentioned, a solution to yield the functions $u = f(x, y)$ and $v = g(x, y)$ which satisfy equations (1) and (2) is not available for the flow over some arbitrary body. Two solutions which are available and are of interest here are the Blasius flat plate problem (9, p. 234-241) and the Rheinboldt suction distribution problem (14, p. 53-54). In the first the boundary layer is developed over a flat plate in which the velocity gradient dU/dx is everywhere zero. This solution is of interest because it is used by Head in the development of his family of boundary layer profiles for use in an approximate method of

solution. This approximate method is what is used in this thesis, and it will be described in a later section. In the second the development of the boundary layer over several shapes in which a certain distribution of suction has been specified is obtained. This solution is of interest because Head's approximate method has been applied to the flow for which Rheinboldt obtained an exact solution. In this manner the results of Head's method can be compared with the results obtained by Rheinboldt to ascertain the accuracy of Head's method for this particular flow.

III. MOMENTUM INTEGRAL RELATION

Earlier mention was made of an approximate method involving the momentum integral relation. The momentum integral relation is a useful application of the momentum theorem of fluid mechanics to a control volume whose boundaries extend through the boundary layer. This momentum integral relation was first devised by T. von Karman and often bears his name (8, p. 1). The flux of mass and momentum through the boundaries of the control volume are obtained by integration over the velocity profile at the boundaries of the control volume. This relation is useful in that we have only to deal with the integrated effect of the velocity profile over the boundary layer rather than the individual components of velocity within the boundary layer. This constitutes a considerable simplification and leads to an approximate technique, such as the Pohlhausen method or, more particularly, the method of this thesis.

The momentum integral relation can be obtained in two ways. The momentum theorem of fluid mechanics can be applied to a control volume which encompasses a portion of boundary layer and whose thickness is greater than that of the boundary layer, as was mentioned, or, alternatively, the boundary layer equations can be integrated directly over the thickness of the boundary layer. These two

derivations appear in Appendix A. The momentum integral relation for steady, two-dimensional, incompressible flow is as follows:

$$\mu \left(\frac{\partial u}{\partial y} \right)_o = \rho \frac{\partial}{\partial x} (U^2 \theta) + \rho U \frac{dU}{dx} \delta^* \tag{3}$$

The integrated effect terms are θ and δ^*.

$$\theta = \int_o^\delta \frac{u}{U} \left(1 - \frac{u}{U} \right) dy \qquad \text{momentum thickness}$$

$$\delta^* = \int_o^\delta \left(1 - \frac{u}{U} \right) dy \qquad \text{displacement thickness} \tag{4}$$

As was mentioned the momentum integral relation finds application in Pohlhausen type solutions.

Pohlhausen Method

Pohlhausen's method (12, p. 1) and (11, p. 232-237) is to generate a family of velocity profiles using a fourth order polynomial as follows:

$$u/U = A(\eta) + B(\eta)^2 + C(\eta)^3 + D(\eta)^4$$

where $\eta = y/\delta$. By specifying the boundary conditions

$$\text{at } y = 0, \quad u = 0$$

$$y = \delta, \quad u = U, \quad \frac{\partial u}{\partial y} = 0, \quad \frac{\partial^2 u}{\partial y^2} = 0$$

and by evaluating the boundary layer equation at the surface to obtain

the relationship

$$\text{at } y = 0, \quad \mu \frac{\partial^2 u}{\partial y^2} = \frac{dP}{dx} = -\rho U \frac{dU}{dx} \tag{5}$$

(Equation (5) will later be referred to as the first compatibility condition at the surface)

the constants A through D can be evaluated in terms of a parameter λ, called the Pohlhausen parameter.

$$\lambda = \frac{\delta^2}{\nu} (dU/dx)$$

$$u/U = (2 + \tfrac{\lambda}{6})\,\eta - \tfrac{\lambda}{2}\,\eta^2 + (-2 + \tfrac{\lambda}{2})\,\eta^3 + (1 - \tfrac{\lambda}{6})\,\eta^4 \tag{6}$$

What has resulted is a one-parameter family of velocity profiles, such that given any value of λ the function ($u/U = f(\eta)$) is determined. At flow separation, (that is, $\left(\frac{\partial u}{\partial y}\right)_o = 0$), λ equals minus twelve ($\lambda = -12$). For λ less than minus twelve ($\lambda < -12$) u/U becomes negative as shown in Figure 1. For λ greater than plus twelve ($\lambda > +12$) we find that the maximum value of u/U is greater than one, as shown in Figure 1, and we do not choose to consider profiles with this characteristic. We can see, then, that all the significant members of the family lie in the range ($-12 \leqslant \lambda \leqslant +12$). Figure 1 shows the approximate shape of the significant members of Pohlhausen's polynomial profiles.

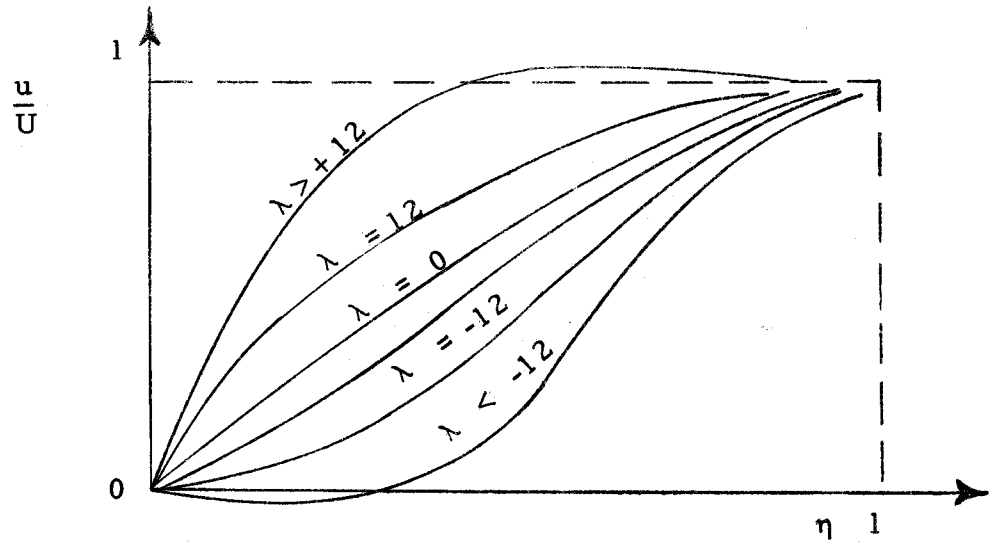

Figure 1. Pohlhausen's polynomial profiles.

Now to use this family of velocity profiles in the momentum integral relation we evaluate the functions θ and δ^* by using equation (6) in equations (4), and we evaluate the term $\mu\left(\frac{\partial u}{\partial y}\right)_o$ from equation (6) and insert these values into the momentum integral relation (3). After some manipulation an ordinary differential equation with δ^2/ν as the dependent variable results. The equation involves U and dU/dx, so that the solution of a particular problem requires that the potential velocity distribution over the surface be known.

The above procedure has been done, for example, to determine the development of the boundary layer over a circular cylinder

and the results appear, along with a comparison with the results of an exact method, in Schlichting (15, Figure 12.8).

The Pohlhausen solution is not what is used in this thesis, but the method of generating a family of profiles and then applying an integral relation to determine the distribution of profiles along the surface is used. I have, therefore, gone into some detail in discussing the Pohlhausen method. What is important to notice in this method for our later discussion of Head's method is that a one-parameter family of velocity profiles is chosen. We make the assumption that each profile in the boundary layer is satisfactorily represented by a member of the family. We, then, satisfy the momentum integral relation to determine the value of the one parameter along the surface of the body under consideration. The shape of the body enters the equation by our choice of the velocity U and the derivative of the velocity dU/dx. The only reason that we say that the Pohlhausen method is approximate is that in a real flow situation it is highly unlikely that the velocity profiles are precisely members of the assumed family. If, however, we were able to devise a flow situation in which all of the velocity profiles were members of Pohlhausen's family, then Pohlhausen's solution ($\lambda = f(x)$) would be the exact solution.

The accuracy, and hence the usefulness, of a method of this type lies in the flow situation being studied. If the profiles which

exist in a certain flow situation are closely approximated by members of the assumed family, then the method is very useful since solutions can be obtained without much difficulty; if, on the other hand, the profiles in a real flow situation are not closely approximated by members of the assumed family, then the method breaks down and the solutions are not useful. The reader should notice at this point the possibility of improving the Pohlhausen method in situations where the real profiles are not reasonably approximated by a polynomial.

In the method of Head which is to be discussed in the following section the flow situations involve the use of suction through the surface of the body, and solutions are desired to be accurate near the point of flow separation. The typical profiles encountered are considerably different in shape from the profiles in Pohlhausen's family. Head devises a new family built from the numerical values of three profiles obtained from exact solutions of the boundary layer equations. The use of this new family greatly improves the usefulness of Pohlhausen's technique, since the number of flow situations satisfactorily handled is extended to include suction profiles and the profiles near separation.

To attain this extended family, however, two parameters are used to specify a given profile instead of just one in the Pohlhausen family. This requires that an additional equation be satisfied to

determine the distribution of the two parameters over the surface of the body in the direction of flow. Head uses an additional integral relation, the energy integral relation, in addition to the momentum integral relation and the first compatibility condition at the surface. This additional equation will be discussed in the next section.

IV. THE METHOD OF HEAD

As was mentioned Head's method is an extension of the method of Pohlhausen. Pohlhausen's one-parameter family of velocity profiles generated from a fourth degree polynomial has been replaced by a two-parameter family generated from the numerical values of three profiles determined from exact solutions. This family is considerably extended in that it includes profiles typical of those for suction and near separation. The derivation of Head's equation and the velocity profile family appear in Head's original paper (4, p. 1-53). What follows is a description based on Head's paper.

Family of Velocity Profiles

To obtain an extended range of profiles the principle is used to adopt a basic profile and modify this by adding varying amounts of two other functions so that the velocity profile function is of the form

$$u/U = f_1(\eta) + c\, f_2(\eta) + d\, f_3(\eta) \qquad (7)$$

The basic profile is f_1 and varying amounts of f_2 and f_3 are added by choosing the appropriate values for c and d. The basic profile f_1 is the Blasius flat plate profile which was mentioned in a previous section. This profile is sketched in Figure 2. The functions f_2 and f_3

are as yet undetermined but may be expected to be similar to the f_2 and f_3 in Figure 2. As shown f_2 and f_3 are chosen to be such that $f_2''(0)$ and $f_3'(0)$ both equal zero. A characteristic of the Blasius profile is that $f_1''(0)$ equals zero.

$$f_2''(0) = f_3'(0) = f_1''(0) = 0$$

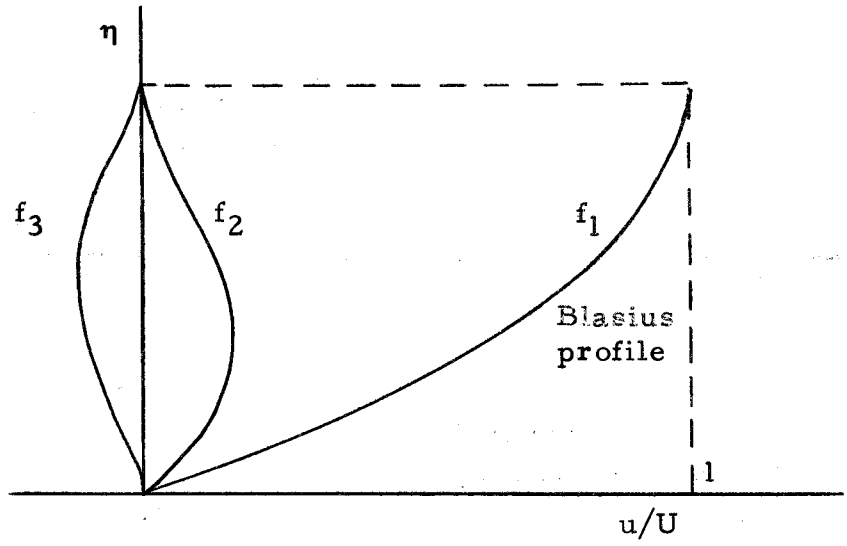

Figure 2. Head's basic and modifying profiles

The functions f_2 and f_3 will now be determined in such a way that two profiles given by equation (7) can be fitted exactly (when c and d are given the appropriate values) to two profiles known from an exact solution of the boundary layer equations. We will refer to these known profiles as $F(\eta)$ and $G(\eta)$

$$F(\eta) = f_1(\eta) + c_1 f_2(\eta) + d_1 f_3(\eta)$$
$$G(\eta) = f_1(\eta) + c_2 f_2(\eta) + d_2 f_3(\eta) \qquad (8)$$

We can see immediately an improvement over the Pohlhausen family in that three profiles in this new family are precisely profiles obtained from an exact solution, that is, when $c = d = 0$ in equation (7) we have the Blasius flat plate profile when $c = c_1$, $d = d_1$ we have the profile $F(\eta)$, and when $c = c_2$, $d = d_2$ we have the profile given by $G(\eta)$.

The following technique is used to obtain f_2 and f_3. As indicated in equations (8), c and d must be assigned the values c_1, c_2, d_1, and d_2 to determine the functions f_2 and f_3. An alternative method to determine f_2 and f_3 is to assign some value to a point on a derivative of f_2 and f_3 which will thereby determine the values c_1, c_2, d_1, and d_2. To demonstrate how this is done, assign arbitrary values to $f_2'(0)$ and $f_3'(0)$, then c_1, c_2, d_1, and d_2 can be determined from the following equations:

$$F'(0) = f_1'(0) + c_1 f_2'(0)$$
$$F''(0) = d_1 f_3''(0)$$
$$G'(0) = f_1'(0) + c_2 f_2'(0) \qquad (9)$$
$$G''(0) = d_2 f_3''(0)$$

These equations readily follow from equations (8) and the fact that we

chose

$$f_2'(0) = f_3''(0) = 0$$

and $f_1''(0) = 0$ in the Blasius profile.

Having determined the values of c_1, c_2, d_1, and d_2 from equations (9) or having assigned these values as in the former alternative we can proceed to determine f_2 and f_3 by choosing some value of η (say $\eta = \eta_1$) and writing

$$F(\eta_1) = f_1(\eta_1) + c_1 f_2(\eta_1) + d_1 f_3(\eta_1)$$

$$G(\eta_1) = f_1(\eta_1) + c_2 f_2(\eta_1) + d_2 f_3(\eta_1)$$

We have two simultaneous linear equations in two unknowns. These can be solved for the unknown points $f_2(\eta_1)$ and $f_3(\eta_1)$, then by choosing sufficient values for η the functions f_2 and f_3 can be given in numerical form.

Head calculated f_2 and f_3 with two different choices of the known profiles $F(\eta)$ and $G(\eta)$. The functions f_2 and f_3 were first calculated using two separation profiles given by Thwaites, and then f_2 and f_3 were again calculated using the asymptotic suction profile* and a hypothetical profile having the same value of $(1/U)(\partial u/\partial \eta)_o$ but with $(1/U)(\partial^2 u/\partial \eta^2)_o = 0$. These two sets of $F(\eta)$ and $G(\eta)$ gave, essentially, two families, one for near separation profiles and one for high skin friction profiles.

* The asymptotic suction profile is the exact solution of the boundary layer equations for the flow over a flat plate with suction.

To obtain f_2 and f_3 from the asymptotic suction profile c_1 and d_1 were arbitrarily given the value one. Then, because of the relationship just mentioned between the asymptotic suction profile and the hypothetical profile, c_2 equals c_1 ($c_2 = c_1 = 1$) and d_2 equals zero. Now, to obtain f_2 and f_3 from the separation profiles (using the second alternative method) c_1, c_2, d_1, and d_2 were determined by setting

$$f_2'(0)_{\text{separation profile}} = f_2'(0)_{\text{asymptotic suction profile}}$$

$$f_3''(0)_{\text{separation profile}} = f_3''(0)_{\text{asymptotic suction profile}}$$

when this is done c_1 and c_2 are calculated to be (-0.493). Functions f_2 and f_3 have, then, been calculated for profiles with high skin friction ($c = 1$) and for profiles with zero skin friction ($c = -0.493$). Functions f_2 and f_3 can be determined for intermediate profiles by using a value of c between 1 and -0.493. Head determines f_2 by interpolation linearly with c between the high friction and the separation profile as shown in Figure 3. A similar figure would be drawn to interpolate for f_3.

The family of velocity profiles has become more complicated than would appear at first glance at equation (7), since the functions f_2 and f_3 are functions not only of η but also of c, where the functional relationship of f_2 with c is given in Figure 3. Nevertheless, we still have a two parameter family, that is, for an arbitrary choice of the

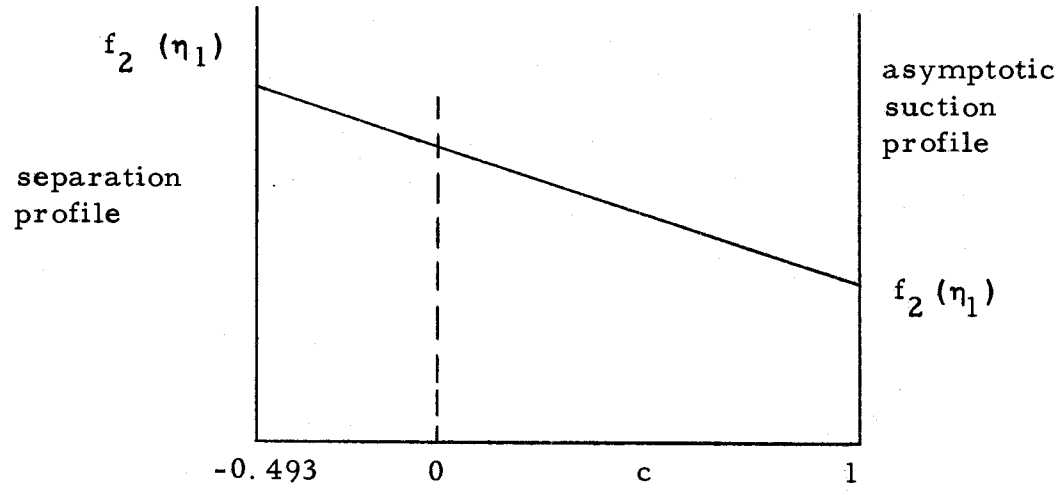

Figure 3. Interpolation of f_2.

constants c and d a single profile is specified. The motivation in settling upon a more complicated relationship is that the resulting family contains members which more closely fit profiles known from an exact solution of the boundary layer equations or by experimental measurement.

The family of velocity profiles is, finally, built up by giving c a series of values; for each of which f_2 is determined as in Figure 3 and f_3 by a similar figure. A series of values for d is chosen and the profiles follow from equation (7).

Later in this discussion of Head's method, equations will be presented in the form in which they are to be used. We will see that the velocity profiles generated above are not required explicitly, but the following integrals of the velocity profile are required.

$$\delta^* = \int_0^\delta \left(1 - \frac{u}{U}\right) dy \qquad \text{displacement thickness}$$

$$\theta = \int_0^\delta \frac{u}{U}\left(1 - \frac{u}{U}\right) dy \qquad \text{momentum thickness}$$

$$\epsilon = \int_0^\delta \frac{u}{U}\left(1 - \left(\frac{u}{U}\right)^2\right) dy \qquad \text{energy thickness}$$

These are obtained from the resulting profiles by numerically evaluting the integrals using equation (7).

We have developed a two-parameter family of velocity profiles and called the independent parameters c and d as in equation (7). In the equations of Head's method the first and the second derivative of the velocity profile at the surface appear. Head introduces convenient dimensionless notation and defines two new parameters to represent these derivatives. The first is labeled ℓ ($\ell = (\theta/U)(\partial u/\partial y)o$) and the second is labeled m ($m = (\theta^2/U)(\partial^2 u/\partial y^2)o$). We will see that in charting properties of the profile shape, (for example, $H = \delta^*/\theta$), that the symbols c and d are no longer used, but ℓ and m have been adopted as the independent parameters of the family.

Head's method requires three relationships to be satisfied. They are the momentum integral relation, the energy integral relation, and the first compatibility condition at the surface. The momentum and energy integral equations are as follows, and their derivation appear in Appendix A and B.

Momentum integral equation:

$$\frac{d\theta}{dx} = \frac{\nu}{U^2}\left(\frac{\partial u}{\partial y}\right)_o - (H+2)\frac{\theta}{U}\frac{dU}{dx} - \frac{v_s}{U}$$

Energy integral equation:

$$\frac{d(U^3\epsilon)}{dx} = 2\nu\int_o^\delta \left(\frac{\partial u}{\partial y}\right)^2 - v_s U^2$$

The momentum integral relation is modified by the introduction of convenient dimensionless notation and becomes

$$t^{*\prime} = \frac{2}{U}\{\ell - \Lambda(H+2) - \lambda\} \qquad (10)$$

The energy integral equation is modified so that the rate of change of the form parameter H_ϵ ($H_\epsilon = \epsilon/\theta$) is given explicitly. In final form with dimensionless notation it is

$$H_\epsilon' = \frac{1}{U t^*}\left[2D^* - H_\epsilon\{\ell - \Lambda(H-1) - \lambda\} - \lambda\right] \qquad (11)$$

where

$$t^* = \left(\frac{\theta}{c}\right)^2 \frac{U_o c}{\nu}$$

$$D^* = \int_o^{\delta/\theta}\left(\frac{\theta}{U}\right)^2\left(\frac{\partial u}{\partial y}\right)^2 d\left(\frac{y}{\theta}\right)$$

and the primes denote differentiation with respect to $\bar{x}$. The first compatibility condition at the surface is the boundary layer equation evaluated at the surface and in dimensionless notation becomes

$$m = -(\Lambda + \ell\lambda) \qquad (12)$$

Equations (10), (11), and (12) form the basis of Head's method.

The parameters λ and Λ are associated with the value of the local suction velocity, and the velocity gradient at the outer edge of the boundary layer, which are the prescribed boundary conditions for a given problem. They are defined as follows:

$$\begin{aligned} \Lambda &= t^* \, d\overline{U}/dx \\ \lambda &= \sqrt{t^*} \, v_s^* \end{aligned} \tag{13}$$

The terms H_ϵ, H, and 2D* are properties of the profile shape and once the family of boundary layer profiles is chosen these properties can be determined for any choice of ℓ and m, the two independent boundary layer profile parameters. Figures 21, 22, and 23 are charts of these properties as functions of ℓ and m.

Step by Step Procedure

The following is a step-by-step procedure to calculate the development of the boundary layer using Head's method. A particular problem, (for example, the flow over a circular cylinder), requires that you first obtain the potential flow solution over the object to obtain the distribution of velocity U and velocity gradient dU/dx outside the boundary layer. Also, we must specify the distribution of suction through the surface of the airfoil. With the boundary conditions set we need to know the boundary layer profile shape at one

point on the airfoil. Head's method will yield the profile shape at every other point. With ℓ and m initially chosen, H_ϵ, H, and 2D* can be read from Figure 21, 22, and 23 respectively. Now the momentum integral equation and the energy integral equation are used to determine the rate of change of t* and H_ϵ respectively, (see equations (10) and (11)). Using the approximation

$$t^*_{\bar{x}+\Delta\bar{x}} = t^*_{\bar{x}} + (dt^*/d\bar{x})(\Delta\bar{x})$$

$$H_{\bar{x}+\Delta\bar{x}} = H_{\epsilon\bar{x}} + (dH_\epsilon/d\bar{x})(\Delta\bar{x})$$

for some selected value of $\Delta\bar{x}$ we know the value of the parameters t* and H_ϵ at the point $\bar{x}+\Delta\bar{x}$. We can now determine the value of ℓ and m at the point $\bar{x}+\Delta\bar{x}$ as follows: determine λ and Λ from t* using equations (13), and insert these values into the first compatibility condition at the surface (equation (12)). This will plot as a straight line on the ℓ-m plane. Plot this line on Figure 21 which is the chart of H_ϵ versus ℓ and m. We are able to find the intersection of this straight line and the constant H_ϵ line as determined from the energy integral relation (equation (11)). This point of intersection determines the value of ℓ and m, and with these values H and 2D* can be read from Figures 22 and 23 respectively. As before we are able to again use the momentum and energy integral equations and determine the profile shape at a point $\Delta\bar{x}$ further downstream.

The point of separation occurs when the parameter ℓ becomes

negative, since the ℓ parameter is a measure of the slope of the profile at the surface. In general the parameter ℓ will begin at a value of about 0.3 or 0.4 at a point on the surface remote from separation and will approach zero as the point of separation is approached. This can be seen from the results of a calculation which will be presented later. If the suction is sufficient to prevent separation the rear stagnation point value will be reached in the calculation without the value of ℓ becoming negative.

The discussion in this section has essentially been based on Head's paper. A more thorough discussion of the derivation of the family of profiles and the use of the equations can be found in the original paper (4, p. 1). The object of this thesis is to use this method to determine the development of the boundary layer profiles about a circular cylinder with suction. The following section will discuss the application of this method to the specific problem, as well as, adapting the method to the digital computer.

V. ADAPTATION OF HEAD'S METHOD TO THE DIGITAL COMPUTER

In the previous section the method of Head was discussed, and the use of the equations with Figures 21, 22 and 23 were described. It was initially found that when this method was applied to the flow over a circular cylinder the calculation diverged, irrespective of where on the cylinder the calculation was begun, that is, the changes in the parameter H_ϵ from one point in the calculation to another became excessively large, and soon the values of the parameters H_ϵ and t* were no longer in the range covered by Figure 21. I am still not fully sure why the calculation initially diverged, but by devising a means whereby the charts were read accurately enough so that small changes in the parameters H_ϵ and t* led to corresponding changes in the other parameters read from the charts, and using small increments over the surface the method was found to yield satisfactory results.

One difficulty in performing the calculations occurred in the region of the stagnation point where the potential velocity was near zero. In the momentum and energy integral equations the term $\overline{U}$ appears in the denominator. The numerator contains several terms which are made up of chart readings (see equations (10) and (11)). If

errors exist in these chart readings or if the starting profile was in error the effect on $t^{*\prime}$ and H_{ϵ}' will be magnified by the division by the small velocity. Head discusses this difficulty and suggests that the increments along the surface of the airfoil be kept very small. To avoid this difficulty the calculation of the solid boundary problem was started at an angle of twenty degrees ($\phi = 20^{\circ}$) where the angle ϕ is measured from the most forward point on the cylinder (see Figure 20), and the starting boundary layer profile (at $\phi=20^{\circ}$) was taken from the exact solution reported in Schlichting (13, Figure 12.8).

The step-by-step procedure of Head's method was described in the previous section, and it will be recalled that the calculations were repetitive, that is, first the parameters were read from the charts, then equations (10) and (11) were used to get $t^{*\prime}$ and H_{ϵ}' respectively, then the compatibility condition at the surface was used to determine the straight line which intersected with the constant H_{ϵ} line which appears in Figure 21. This allowed the charts to be read again and the calculation to proceed at a slightly increased position on the surface of the airfoil. When the increments were kept small the calculations became quite laborious, and the advantage of using a computer became apparent. If the calculations could be programmed and the charted information stored in the memory of the machine, the determination of the development of the boundary layer profiles over

a circular cylinder with various suction distributions would be a comparatively simple matter.

The greatest difficulty in adapting this method to a machine was the problem of handling Figures 21, 22 and 23. Three courses of action were considered. First, three algebraic expressions could be devised which when plotted approximate the charts of H_ϵ, H, and 2D*, second, the information on the charts could be put in the form of tables and the three tables stored in the memory of the machine. The third possibility was to enter, as a table, the three basic profiles that Head used in generating his family of profiles, then write a program which would derive the required profile parameters from the original profiles. This would be essentially re-deriving the family of profiles each time a value from the chart was needed during the calculation.

This third possibility was not thought out in detail primarily because the other two seemed to present less difficulty. The other two possibilities were both tried, and the method chosen was to store the charted information in the memory of the machine in the form of three tables. The writing of the algebraic expressions did work with partial success, however. What was done was to replace the lines of the chart by a series of straight lines. For example, consider the sketch of the H_ϵ chart which appears in Figure 4. Based on the

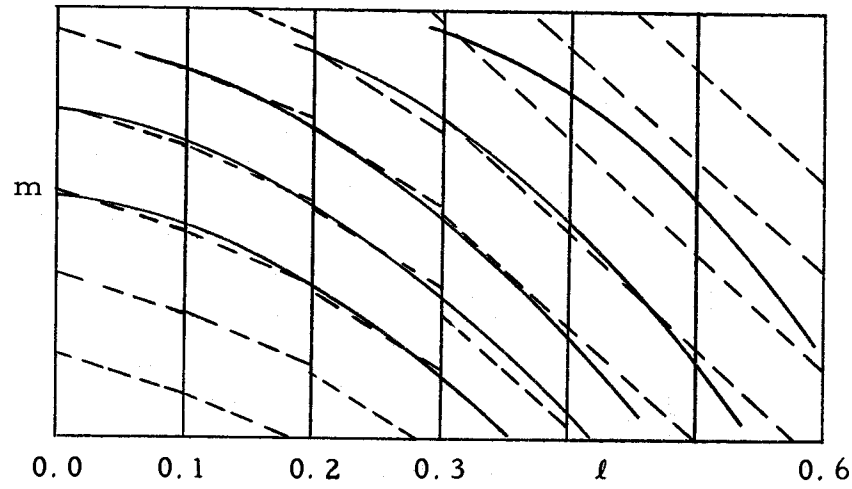

Figure 4. Linear approximation to Figure 21

results of hand calculation it was known, approximately, what ℓ -m path would be followed through the calculation of the solid boundary circular cylinder. The chart was then divided into four zones of ℓ : 0.0 - 0.1, 0.1 - 0.2, 0.2 - 0.3, and 0.3 - 0.6. In each zone the function was taken to be of the form

$$H_\epsilon = a\,\ell + b\,m + c$$

where a, b, and c are constants. By reading the derivative of H_ϵ in the ℓ and m directions and by reading the coordinates of a point on the chart, the constants a, b, and c could be evaluated. This was done independently in each of the four zones, and depending on the zone of ℓ being used during the calculation, the appropriate value of

the constants a, b, and c would be chosen. This linearization was done on each of the three charts.

This method worked quite satisfactorily on the solid boundary problem, but the calculation diverged when this technique was used in a flow situation involving suction. It was later found that several errors existed in the program, but the technique of using linear equations was still dropped because it became evident that the ℓ-m path, and hence the profiles encountered, in a solid boundary problem would be significantly different from the ℓ-m values encountered in a suction problem. Hence, the ℓ-m path followed in future problems could be expected to fall outside the region in which the accuracy of the linear equations was satisfactory. If the use of the linear equation technique was to be continued a "cut and try" procedure would have to be adopted, that is, after a problem had been run the values of H_ϵ, H, and 2D* would have to be compared with those read from the chart for the same values of ℓ and m. If it was found that the values of H_ϵ, H, and 2D* were in significant error the constants a, b, and c would have to be re-calculated for a region around the ℓ-m values actually encountered.

The method settled upon is to enter three tables into the memory of the computer. The first is entered as m as a function of ℓ and H_ϵ [$m = m(\ell, H_\epsilon)$], and the second and third are H and 2D* as functions of ℓ and m [$H = H(\ell, m)$ and $2D^* = 2D^*(\ell, m)$]. It will

be recalled that in using the charts an intersection must be found on the H_ϵ chart between a constant H_ϵ line, determined by the energy integral equation, and a straight line, determined by the first compatibility condition at the surface. When this intersection is found the ℓ and m values determined are used to read H and 2D*.

The following is an explanation of how the three tables were used by the computer program. Consider first the first table, that of $m = m(\ell, H_\epsilon)$, where the intersection must be determined. Figure 5 represents a portion of this H_ϵ chart where the specific entries in the table of ℓ and H_ϵ are indicated. The dashed curve line represents the constant H_ϵ line which is prescribed by the energy integral equation. In the example of Figure 5 it is drawn between $H_{\epsilon 2}$ and $H_{\epsilon 3}$, where $H_{\epsilon 2}$ is the closest entry in the table below H_ϵ and $H_{\epsilon 3}$ is the closest entry in the table above H_ϵ. The straight line d-d is the result of the momentum integral equation and the first compatibility condition at the surface. We must find the intersection of line d-d and the dashed curved line H_ϵ. The technique is to first find the value of ℓ at the intersection of $H_{\epsilon 2}$ and line d-d (call this value ℓ_a), then find the value of ℓ at the intersection of $H_{\epsilon 3}$ and line d-d (call this value ℓ_b), finally use linear interpolation to find the value of ℓ at the intersection of the H_ϵ line and line d-d. This last step

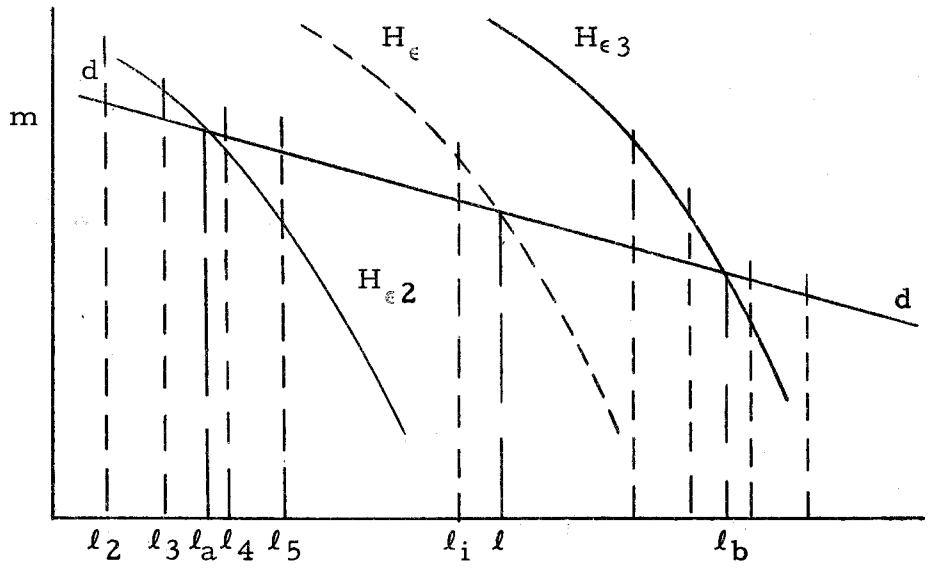

Figure 5. The H_ϵ chart using tabular entries.

is accomplished by the following expression:

$$\ell = \ell_a + \frac{H_\epsilon - H_{\epsilon 2}}{H_{\epsilon 3} - H_{\epsilon 2}} (\ell_b - \ell_a) \qquad (14)$$

To find ℓ_a assume that the algebraic value of the slope of the line d-d is greater than the algebraic value of the slope of the curved line $H_{\epsilon 2}$ near the point of intersection. This is the configuration shown in Figure 5. Choose a value of ℓ in the table and near the desired point of intersection (say ℓ_2), determine the algebraic sign of the following expression:

$$m(\ell_2, H_{\epsilon 2}) - (-\lambda \ell_2 - \Lambda) \qquad (15)$$

where $m(\ell_2, H_{\epsilon 2})$ means the entry in the table for the values $H_\epsilon = H_{\epsilon 2}$ and $\ell = \ell_2$. If the sign of equation (15) is positive

the desired point of intersection lies to the right, as in this example. If it is negative the point of intersection lies to the left, and if it is zero the point of intersection has been found. In this example we would choose a new value of ℓ one interval to the right and again take the difference as in equation (15). To determine if the point of intersection has been crossed take the product of the new difference and the previous difference, which in this example would be

$$[\, m\,(\ell_2,\, H_{\epsilon 2}) - (-\lambda\, \ell_2 - \Lambda)\,]\;[\, m\,(H_{\epsilon 2},\, \ell_3) - (-\lambda\, \ell_3 - \Lambda)\,]$$

Determine the algebraic sign of this product. If it is negative the point of intersection has been crossed, but if it is positive we must proceed to another trial value of ℓ. In this example the intersection occurs between ℓ_3 and ℓ_4. Linear interpolation is used to find the value of ℓ_a between ℓ_3 and ℓ_4 by solving simultaneously for ℓ in these two linear equations.

$$m = \frac{m(\ell_3, H_{\epsilon 2}) - m(\ell_2, H_{\epsilon 2})}{\ell_3 - \ell_2}\, \ell + \left[m(\ell_2, H_{\epsilon 2}) - \frac{m(\ell_3, H_{\epsilon 2}) - m(\ell_2, H_{\epsilon 2})}{\ell_3 - \ell_2}\, \ell_2 \right]$$

$$m = -\lambda\, \ell - \Lambda$$

where the first equation is that of a straight line drawn between the values $m(\ell_3,\, H_{\epsilon 2})$ and $m(\ell_4,\, H_{\epsilon 2})$ and the second equation is the equation of line d-d. This same procedure is repeated at the intersection of the line d-d and $H_{\epsilon 3}$ to determine ℓ_b. When this has been done ℓ is determined from equation (14), as was mentioned. To

determine the value of m substitute the resulting value of ℓ into equation (12).

With ℓ and m determined we may proceed to obtain H and $2D^*$ from the second and third table respectively. Linear interpolation was used in reading these tables. Let ℓ_i and m_i be the nearest lower values in the table to ℓ and m respectively, then H will be given by the following expression:

$$H = H(\ell_i, m_i) + \frac{H(\ell_{i+1}, m_i) - H(\ell_i, m_i)}{\ell_{i+1} - \ell_i} (\ell - \ell_i)$$

$$+ \frac{H(\ell_i, m_{i+1}) - H(\ell_i, m_i)}{m_{i+1} - m_i} (m - m_i)$$

In the same manner

$$2D^* = 2D^*(\ell_i, m_i) + \frac{2D^*(\ell_{i+1}, m_i) - 2D^*(\ell_i, m_i)}{\ell_{i+1} - \ell_i} (\ell - \ell_i)$$

$$+ \frac{2D^*(\ell_i, m_{i+1}) - 2D^*(\ell_i, m_i)}{m_{i+1} - m_i} (m - m_i)$$

This completes the reading of the tables, which gives the values to be used in the momentum and energy integral relations for ℓ, m, H_ϵ, H, and $2D^*$. The terms λ and Λ are evaluated from equations (13) when the potential velocity distribution and the suction distribution have been chosen. The potential velocity distribution, as well

as, the various suction distributions used are presented in the next section. The remainder of the work of adapting Head's method to the digital computer is straightforward programming. Appendix F contains a copy of the Fortran program as well as a flow diagram and a brief description of the details of the program.

VI. FLOW SITUATIONS CALCULATED AND PRESENTATION OF RESULTS

Four different types of suction distribution were used, and they will be presented in this section. The potential velocity distribution, in all cases, was taken to be that of the potential flow over a circular cylinder with the circulation specified. The value of this velocity is given by the expression (see Appendix C)

$$\overline{U} = 2(\sin \phi - \sin \phi s)$$

where the angle ϕ is measured from the most forward point on the cylinder (see Figure 20). The first two suction distributions were used because an exact solution of the boundary layer equations was available for these flows. These first two distributions serve as a check on Head's method, although it should be understood that this check is really valid for these two flow situations only, as the method can get into errors as boundary layer profiles not closely approximated by Head's family are encountered. The third suction distribution was calculated so that the results could be compared with the results of another approximate method, that of Ando, which will be discussed later in this section. Finally, a mathematical model was devised for the suction distribution that occurs on a uniform porosity cylinder. By varying the angle of the rear stagnation point (ϕs), the uniform porosity of the cylinder material, and the uniform internal

pressure of the cylinder a study could be made of the effect of suction on the position of the point of flow separation. These four types of suction distribution, with results, will be considered in order.

Solid Boundary Problem

This is the flow over a circular cylinder in the absence of suction. The point of flow separation has been calculated by exact methods, and this value, as well as the distribution of several boundary layer profile characteristics is given in Schlichting (15, Figure 12.8) and Rheinboldt (14, Figure 15). A plot of this distribution with the corresponding distribution obtained by Head's method is shown in Figures 6, 7, 8 and 10. The parameters used in these figures are those of the corresponding reference, and the numerical results obtained from the computer are shown in Appendix F, Table 3. The point of separation computed by exact methods is $\phi = 110$ degrees as reported by Schlichting (15, p. 136) and $\phi = 109.0$ degrees as reported by Gortler using a Blasius type series (3, p. 1). Gortler's results appear in Curl and Skan (2, p. 262). This same point is reported by Witting (16, p. 396) to be $\phi = 108.9$ degrees using the Blasius-Ulrich method and $\phi = 105$ degrees using the difference method of Gortler. Figure 9 shows the distribution of slopes of the profiles at the surface. The circled points are the values calculated,

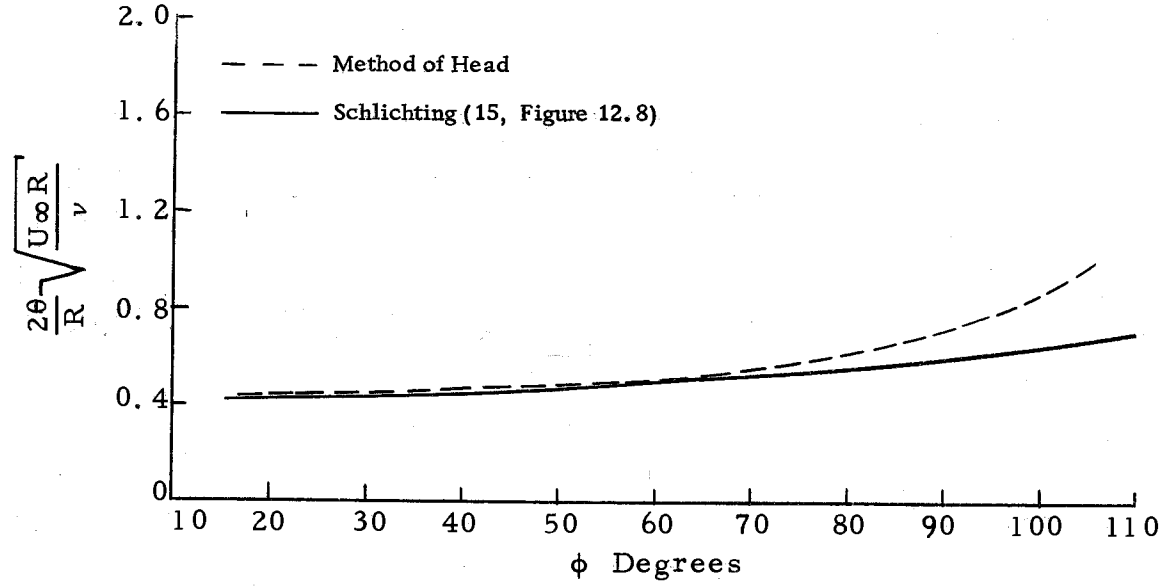

Figure 6. Comparison of momentum thickness with that from Schilchting (solid boundary)

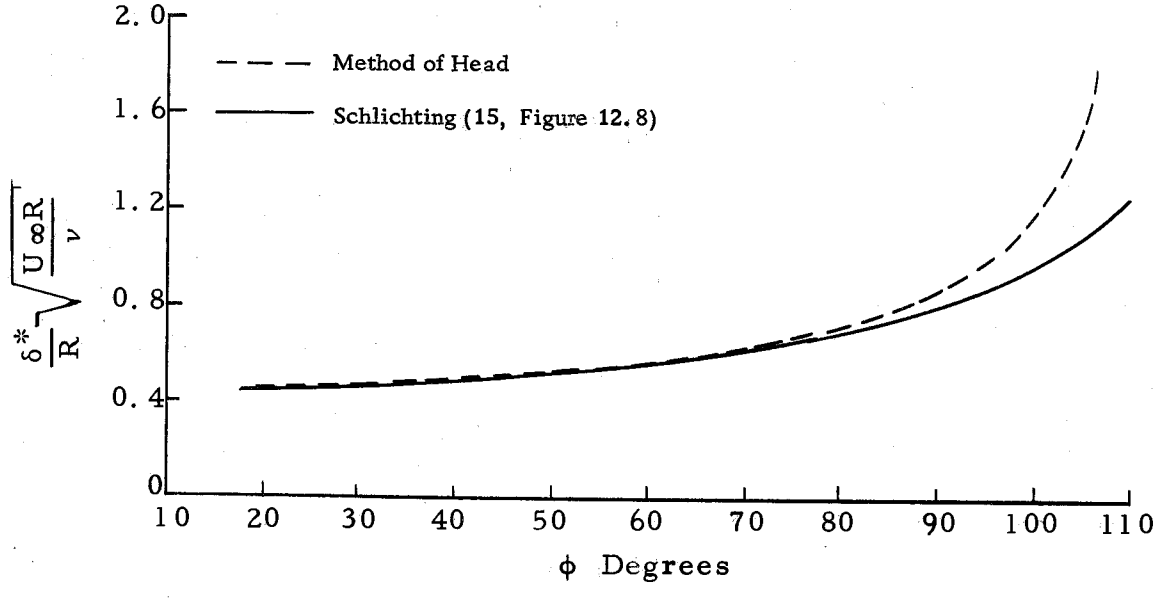

Figure 7. Comparison of displacement thickness with that from Schlichting (solid boundary)

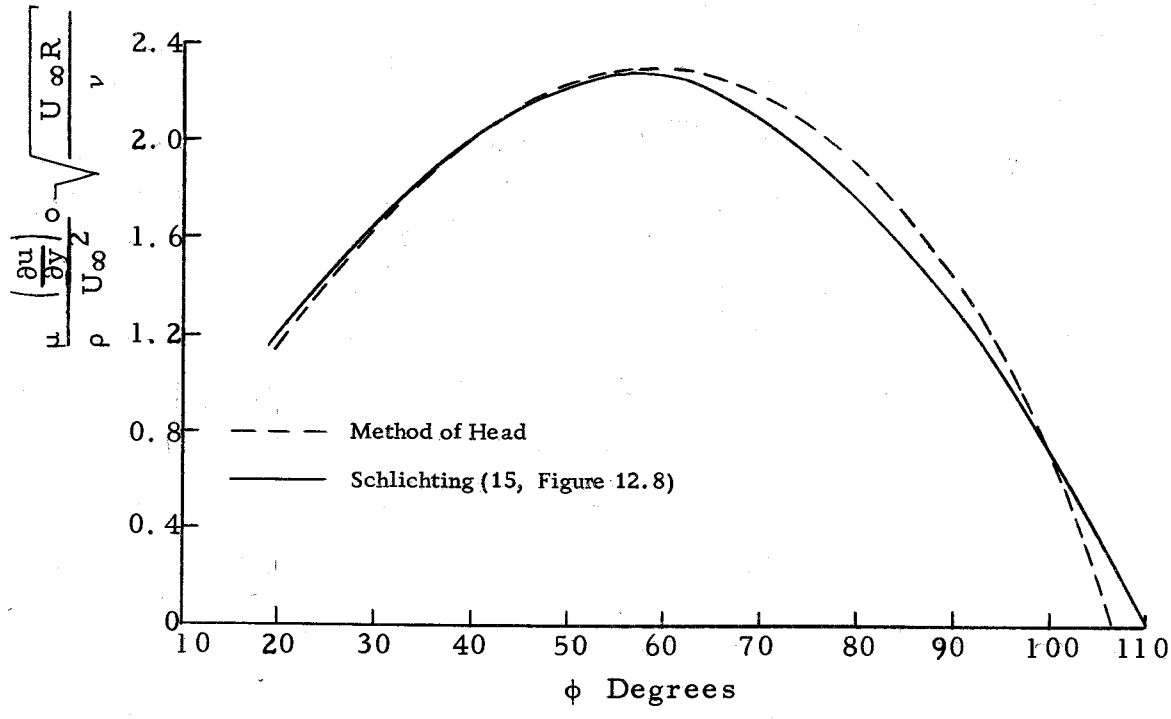

Figure 8. Comparison of the wall shear stress with that from Schlichting (solid boundary)

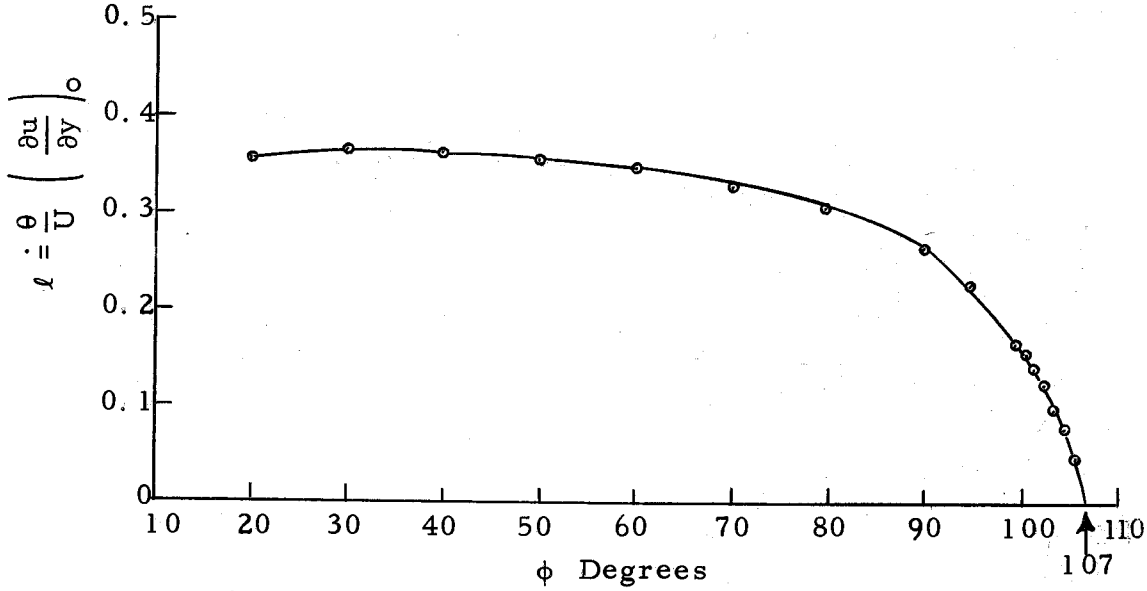

Figure 9. Extrapolation of the slope of the profile at the surface to determine the precise point of separation (solid boundary)

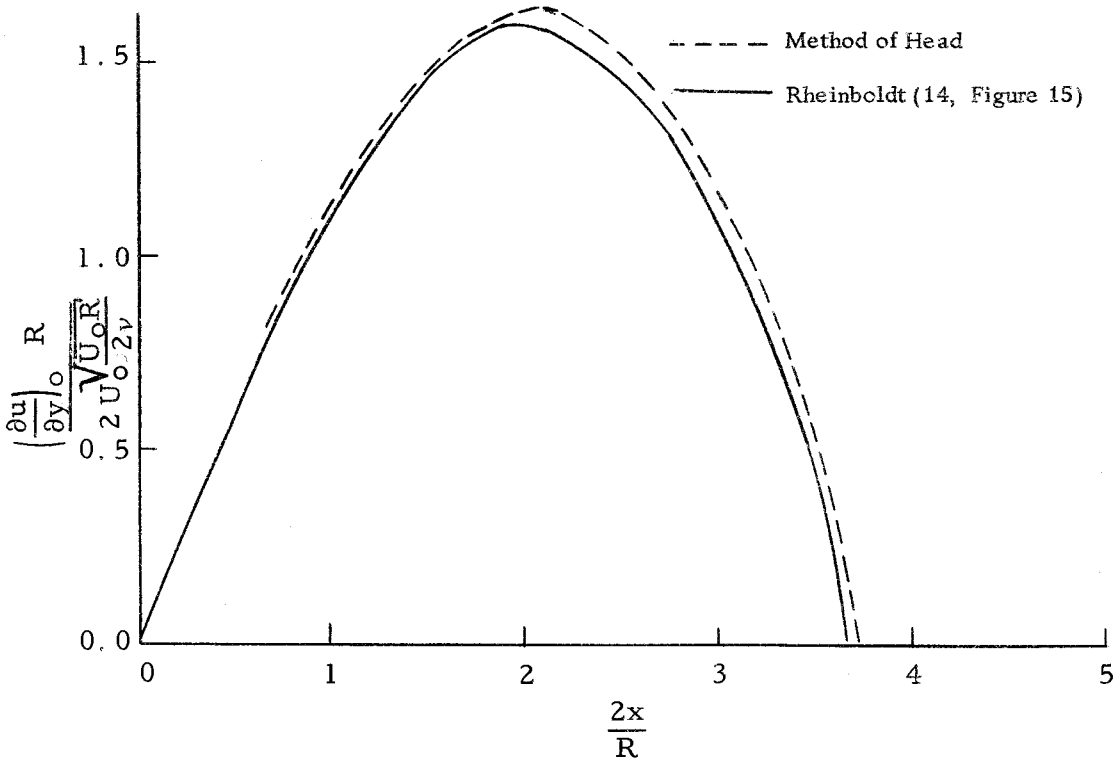

Figure 10. Comparison of the wall shear stress with that from Rheinboldt (solid boundary)

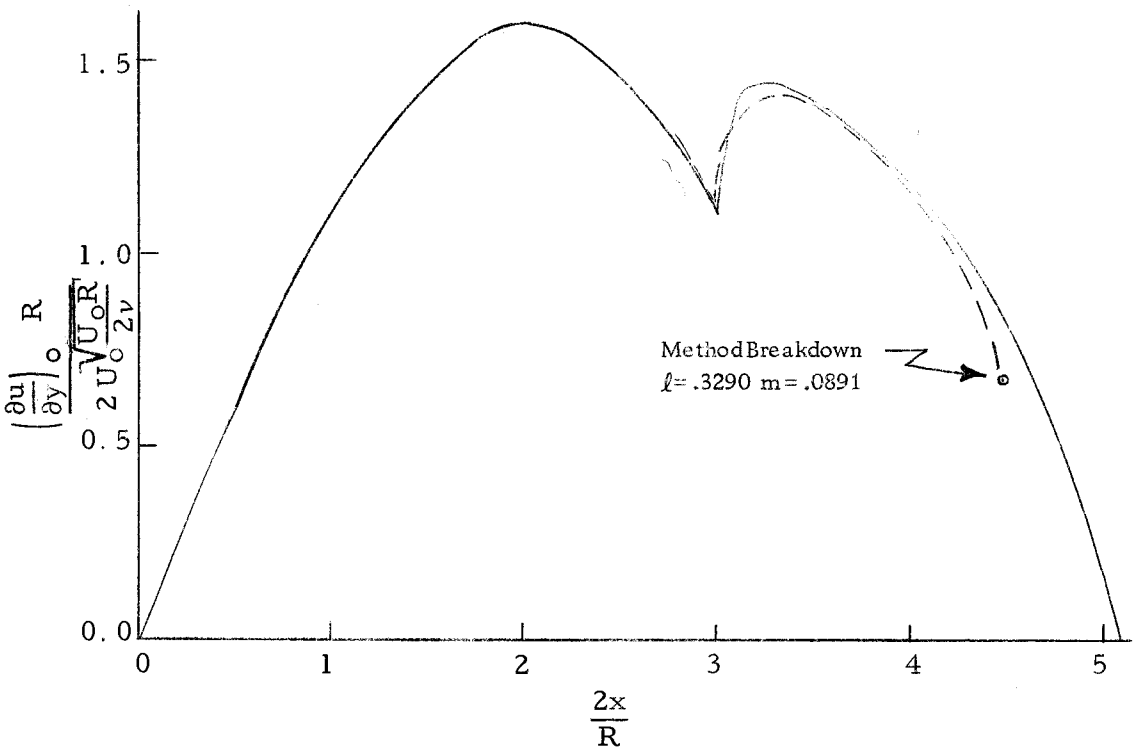

Figure 11. Comparison of the wall shear stress with that from Rheinboldt (Rheinboldt suction distribution)

and the precise value of the point of separation is found by extrapolation as shown. This point of separation, which is the result of Head's method, is seen to be ϕ = 107 degrees. It may be concluded, then, that for this flow Head's method predicts a point of separation comparable to Blasius and difference methods. It might be added that the point of separation shown by the solid line in Figure 10 corresponds to the value reported by Witting.

Rheinboldt Suction Distribution

Here again, the results of an exact method are available (14, Figure 15). The suction distribution specified is shown in Figure 13. Rheinboldt predicts the point of flow separation to be at a value $2x/R$ =5.1 (or ϕ = 146.1 degrees), and the distribution of dimensionless shearing stress at the wall is shown in Figure 11, (along with the distribution obtained with Head's method). Up to $2x/R$ =4.48 (or ϕ = 128.4 degrees) the agreement is found to be good, but the results of Head's method terminate at this point.

One of the conclusions to be brought out later in this thesis is that under conditions of sufficiently high suction and high adverse pressure gradient Head's method will break down, that is, no profile in his family will simultaneously satisfy the momentum integral equation, the energy integral equation, and the first compatibility condition

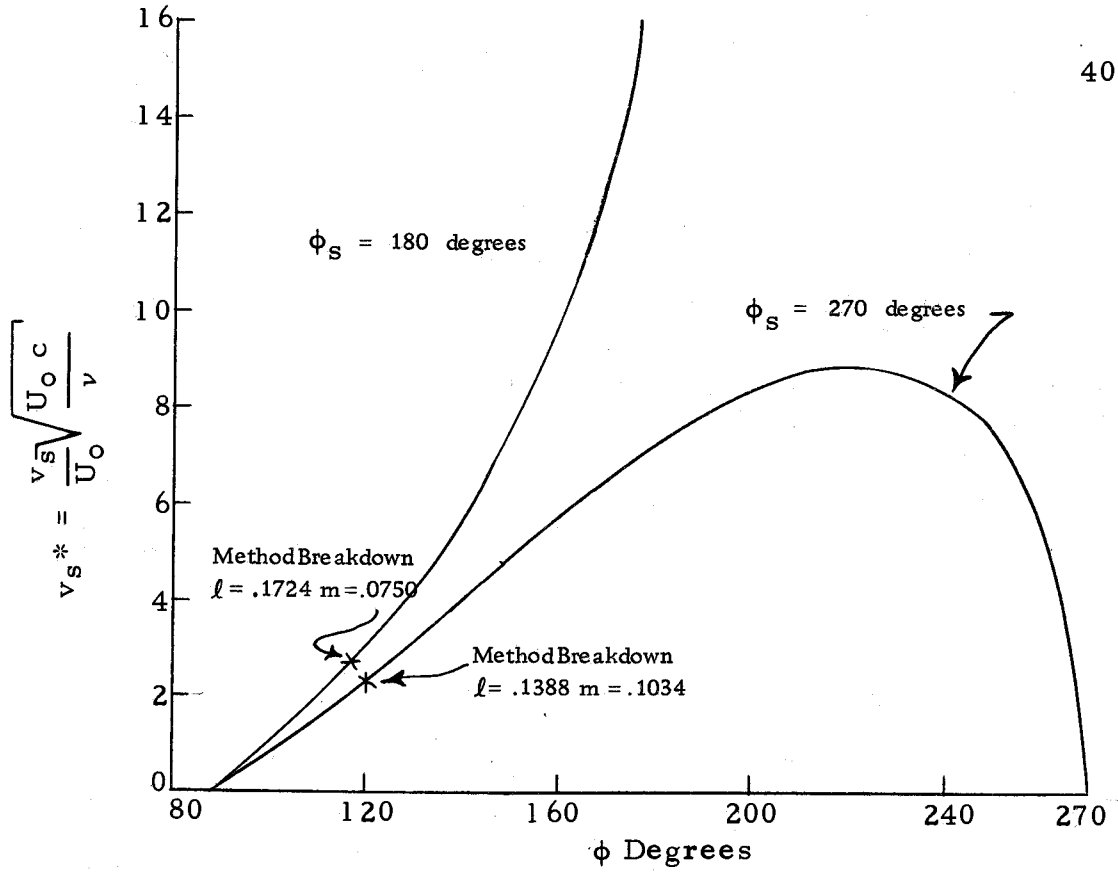

Figure 12. Ando suction distributions showing the point at which Head's method broke down.

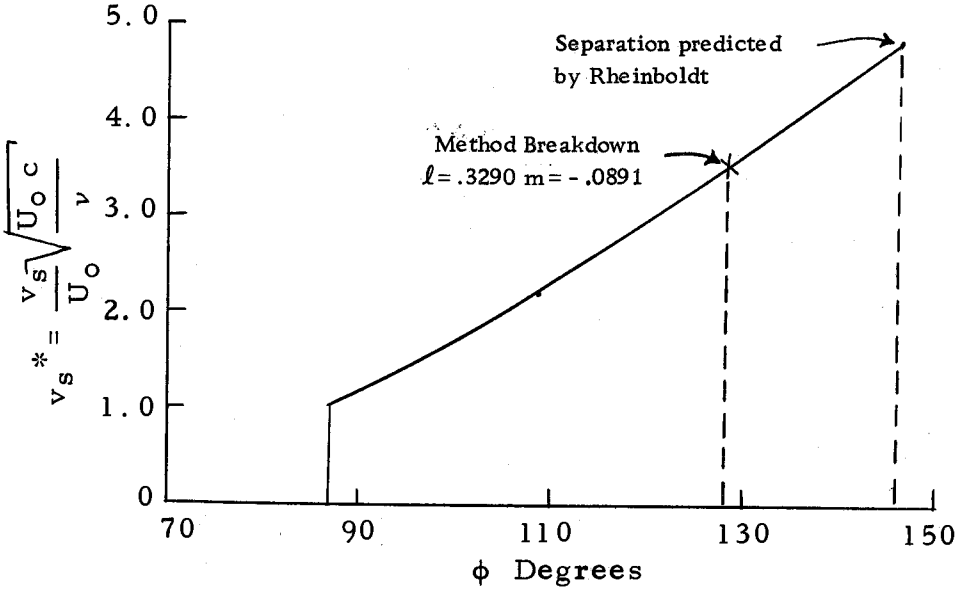

Figure 13. Rheinboldt suction distribution showing the point at which Head's method broke down.

at the surface. It will be recalled from Section V that an intersection was to be found between a straight line determined by the momentum equation and the first compatibility condition at the surface and a constant H_ϵ line as determined by the energy integral equation. When Head's method has broken down there is no intersection. This can be seen by noticing the last calculation of the results appearing in Appendix F, Table 2. Following this step the machine is unable to find an intersection. The explanation of the printed words, "IMPROPER SLOPES", is given in Appendix E. Evidence that there is no intersection is found by continuing the calculation by hand one more step beyond the last step of Table 2. Then by plotting the constant H_ϵ lines from Figure 21 which are just above and just below the H_ϵ line in question, it can be seen that there is no intersection (see Figure 14). This in itself is inconclusive since it has been shown that there is no intersection between line d-d of Figure 14 and the lower H_ϵ line. This does not preclude the possibility that the line d-d does intersect the H_ϵ line in question (not shown of Figure 14). However, by noting that H_ϵ is decreasing $(dH_\epsilon/d\phi < 0)$, and that the increasing adverse pressure gradient tends to shift line d-d up, and that the increasing suction tends to decrease the slope of the line d-d as shown by its equation

$$m = -\sqrt{t^*}\, v_s^* \ell - t^* \overline{U}'$$

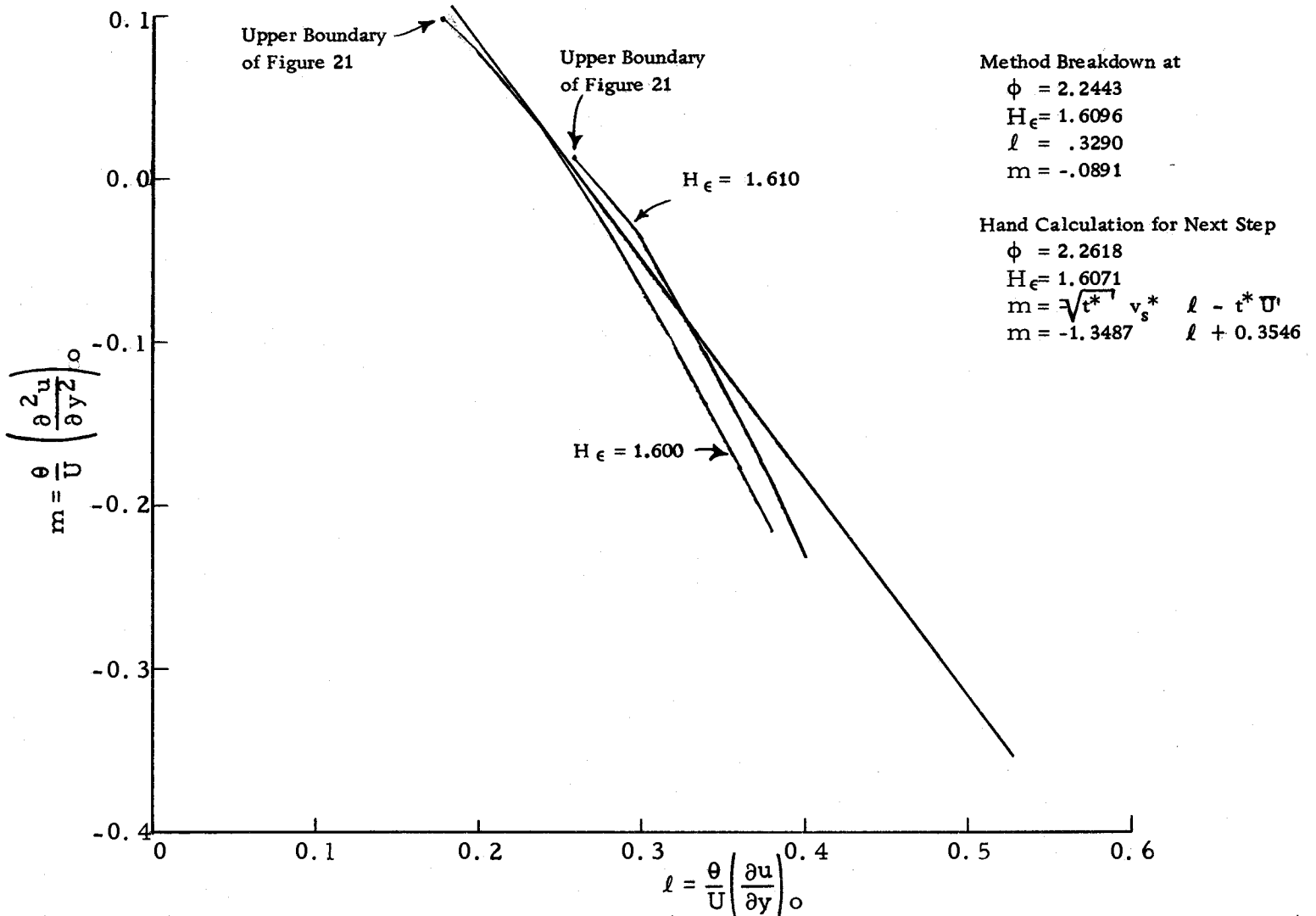

Figure 14. Portion of Figure 21 showing the lack of intersection at the point at which Head's method broke down during the Rheinboldt suction distribution calculation.

it can be seen that the calculation is very near the point at which there is no intersection between the H_ϵ line in question and the line d-d.

It should also be noted in Figure 14 that the point of tangency is near the upper ends of the constant H_ϵ lines. The ends of these lines are the upper boundaries for which data is given in Figure 21. If the calculation had not broken down at this point it would soon have gone off the region in Figure 21 in which data is given. This difficulty will be seen to occur later in this section with the uniform porosity cylinder suction distributions. These two difficulties with Head's method just mentioned will be referred to as the method breakdown and the off chart difficulties respectively. It will be seen on Figures 12, 13, 15, and 16 that the calculations in which one of the above mentioned difficulties were encountered are accordingly marked, and the last boundary profile shape calculated is indicated by giving the appropriate values of ℓ and m.

Ando's Suction Distribution

This suction distribution is obtained by another approximate method which will not be discussed in detail (1, p. 1). The method results in determining the suction distribution necessary to maintain the shape factor (H) at a constant value. It is hypothesized in the method that if H is not permitted to increase the flow will not

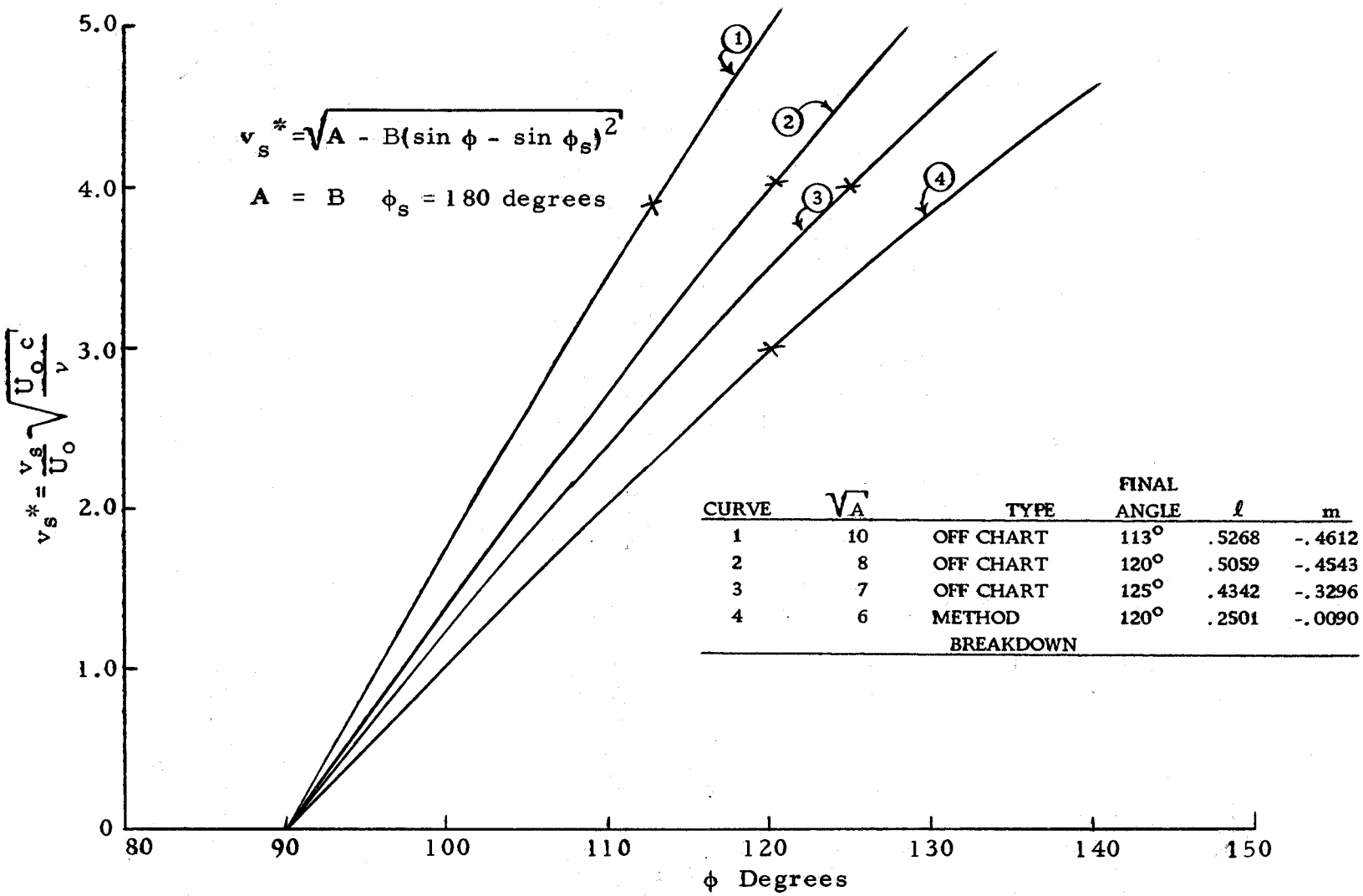

CURVE	$\sqrt{A}$	TYPE	FINAL ANGLE	ℓ	m
1	10	OFF CHART	113°	.5268	-.4612
2	8	OFF CHART	120°	.5059	-.4543
3	7	OFF CHART	125°	.4342	-.3296
4	6	METHOD BREAKDOWN	120°	.2501	-.0090

Figure 15. Uniform porosity cylinder suction distributions for ϕ_s = 180 degrees with the result of each calculation indicated.

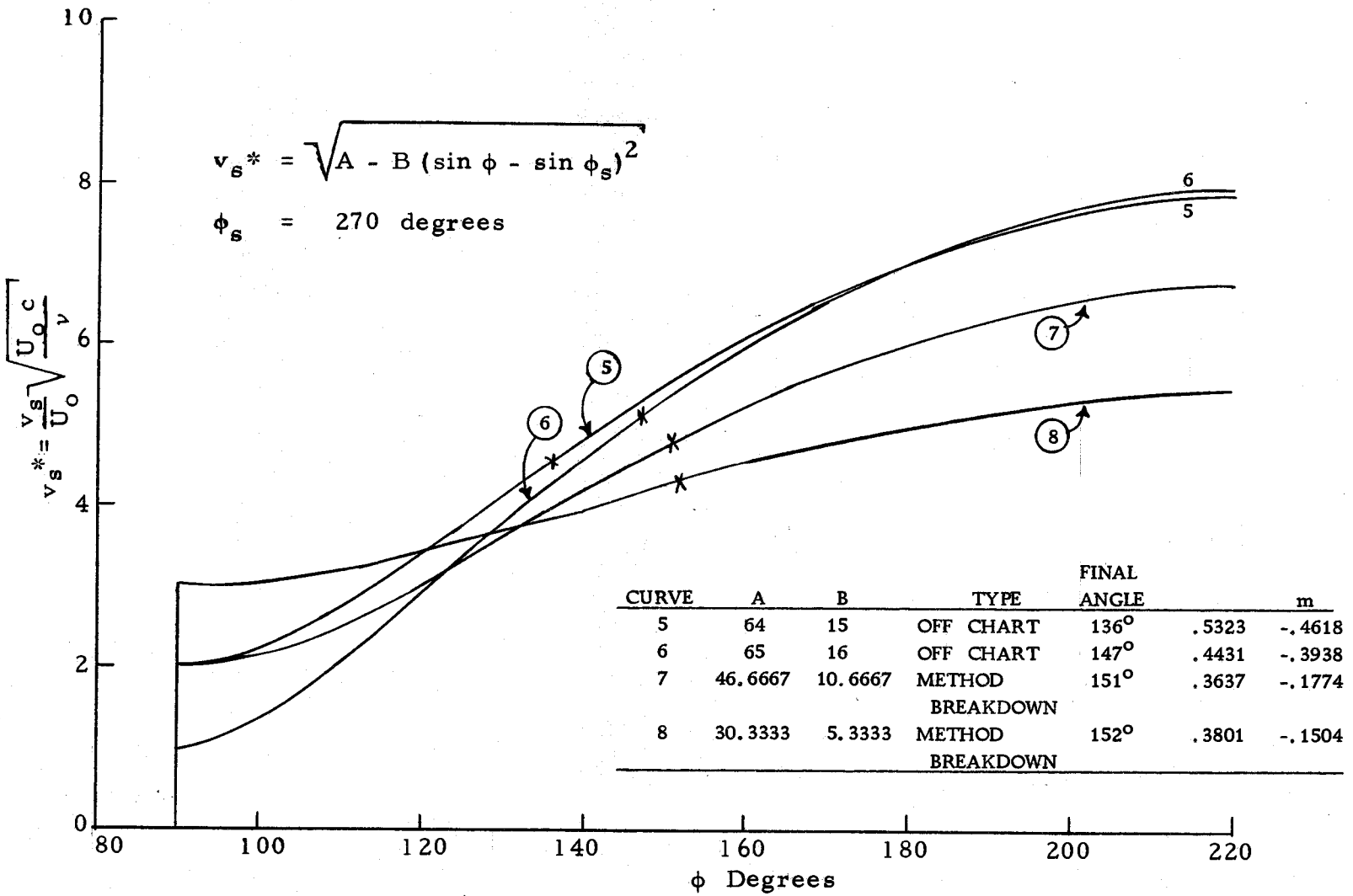

CURVE	A	B	TYPE	FINAL ANGLE		m
5	64	15	OFF CHART	136°	.5323	-.4618
6	65	16	OFF CHART	147°	.4431	-.3938
7	46.6667	10.6667	METHOD BREAKDOWN	151°	.3637	-.1774
8	30.3333	5.3333	METHOD BREAKDOWN	152°	.3801	-.1504

Figure 16. Uniform porosity cylinder suction distribution for ϕ_s = 270 degrees with the result of each calculation indicated.

separate. Two suction distributions are shown in Figure 12, and they are the results of Ando's method for a rear stagnation point angle of $\phi s = 180$ degrees and $\phi s = 270$ degrees. The calculated results appear in Appendix F, Tables 3 and 4. It will be seen that both calculations resulted in a method breakdown. There is good reason to seriously doubt the validity of the results of Ando's method, however, since H did not retain a constant value and the value of ℓ had fallen below $\ell = 0.2$ prior to the method breakdown, which is nearing separation. No further discussion will be given of the results of Ando's suction distribution; it will only be reported that these suction distributions do not appear to be sufficient to maintain attached flow.

Uniform Porosity Cylinder

As mentioned earlier in this section a mathematical model was devised for the suction distribution which would occur on a cylinder with uniform porosity on the back half, that is, one in which the porosity is independent of the angle ϕ except for the discontinuity at the top and bottom. The suction varies along the surface because of the variation of the pressure on the outside of the cylinder and the uniform pressure within the cylinder. This function is derived in Appendix D and is of the form

$$v_s^* = \sqrt{A - B (\sin \phi - \sin \phi s)^2} \quad .$$

Adjusting the parameters A, B, and ϕs corresponds to adjusting the uniform porosity of the cylinder, the rear stagnation point angle and the uniform internal pressure. In all cases the suction velocity was set at zero on the front half of the cylinder ($-90^{\circ} < \phi < 90^{\circ}$) which corresponds to no porosity in this region.

Two different choices of ϕs were used: $\phi s = 180$ degrees and $\phi s = 270$ degrees. In the first choice of the angle ϕs the constant A was taken to equal B. This corresponds to the physical situation in which the outside pressure at the top of the cylinder ($\phi = 90$ degrees) equals the uniform internal pressure. This results in a family of cosine curves of varying magnitude. Four of these suction distributions were calculated, and they appear in Figure 15. with the point to which the calculation proceeded indicated. The ℓ and m values correspond, as before, to the last profile calculated. The results of the second choice of ϕs ($\phi s = 270$ degrees) are shown in Figure 16. Here an attempt was made to tailor the suction distribution, by appropriate choices of A and B, so that the calculation would proceed as far as possible into the adverse pressure gradient. It was noticed that better results were obtained by choosing a high initial suction ($\phi = 90$ degrees) and keeping the magnitude of the resultant suction distribution curve at a lower level. This is approaching a uniform suction situation. The results of each calculation is marked on Figure 16.

VII. CONCLUSIONS AND PROPOSED MODIFICATION OF HEAD'S METHOD

The purpose of this thesis was to apply the method of Head to calculate the development of the boundary layer over a circular cylinder with suction. It was desired to determine if Head's method gave satisfactory results with this pressure distribution, and, if so, the method would be applied as a check on the results of Ando's method. Head's method was found to yield good results with the situation of zero suction velocity, as seen in Figure 6, 7, 8, 9, and 10, and the results were good up to a point with the Rheinboldt suction distribution, as seen in Figure 11.

Two difficulties were encountered which prematurely terminated the calculations. The method broke down, as seen in the Rheinboldt and Ando suction distributions. That is, the calculation proceeded to a point at which it was no longer possible to find a profile in Head's family which satisfied the relationship between the first and the second derivative of the profile at the surface, as determined by the momentum integral equation and the first compatibility condition at the surface and, at the same time, satisfied the value of H_ϵ, as determined by the energy integral equation. The second difficulty labeled "OFF CHART" in the preceding data, was that the first or second derivative of the profile at the surface exceeded the values for

which properties are given in Figures 21, 22, and 23. This difficulty was found with several of the uniform porosity cylinder suction distributions.

Based on these observations it will be concluded that Head's method yields good results when the adverse pressure gradient and the suction are sufficiently low, but the method tends to break down or go off chart as these quantities are increased. With regard to Ando's method, it will be concluded that there is good reason to seriously doubt the validity of its results. This conclusion cannot be more definite, since Head's method broke down prior to separation being indicated using Ando's suction distribution, but the calculation appeared to be progressing toward separation at the point at which Head's method broke down.

It would be desirable to modify Head's method so that the two difficulties mentioned could be overcome. The off chart trouble can be corrected by extending the charted information of Figures 21, 22, and 23 to include more values of ℓ and m. This extension is of limited advantage, for if the family of profiles were overextended the members of the family would no longer accurately represent profiles which appear in real flow situations. The method breakdown trouble can only be corrected by modifying the members of the family of profiles so that they more closely represent the profiles encountered in

the flow situations of this thesis. In Section IV the family of profiles used by Head was presented, and it will be recalled that f_2 and f_3 were chosen such that two profiles known from an exact solution of the boundary layer equations were precisely fitted. Unfortunately, however, it was found that the functions f_2 and f_3 as determined by using near separation profiles were considerably different from functions f_2 and f_3 as determined by using high friction profiles. Head resolved the difficulty by introducing the linear interpolation as shown in Figure 3. It is at this point that I suggest that the family of profiles be modified. This modification would involve using the digital computer.

The basic technique of deriving the family, using linear interpolation, remains unchanged. The modification is that not just two sets of two exact profiles would be used, but several sets which include not only the shapes of the profiles considered by Head, but also the profiles which appear in the condition of high suction and high adverse pressure gradient. These additional sets of known profiles would be chosen from either exact solutions or from experimental measurements. A review of the literature would be required to determine what known profile shapes are available. These additional profile shapes would be used as follows. Instead of using tables in the computer for Figures 21, 22, and 23, the machine would calculate these profiles each time they were needed. The functions f_2 and

f_3, then, would be calculated from two sets of two known profiles taken from the several sets stored in the memory of the machine. The program would include criteria to decide which two sets of known profiles most closely resemble the profiles being encountered in a given flow situation. For example, if this modification were being used with the Rheinboldt suction distribution problem at the point at which the method broke down, the family would be derived using known profiles other than the near separation and high friction profiles used by Head.

It is felt that if this modification were used, the accuracy of Head's method could be preserved, and the method would be extended to apply to the flow situations of this thesis.

BIBLIOGRAPHY

1. Ando, Shigenori. A calculation of distributed suction required to control laminar boundary layer. (Translated in Japan Society of Aero-Space Sciences 2(3):65-71. 1959).

2. Curle, N and S. W. Skan. Approximate methods for predicting separation properties of laminar boundary layers. The Aeronautical Quarterly 8:257-268. August 1957.

3. Görtler, H. A new series for the calculation of steady laminar boundary layer flows. Journal of Mathematics and Mechanics 6:1-66. 1957.

4. Head, M. R. An approximate method of calculating the laminar boundary layer in two-dimensional incompressible flow. Aeronautical Research Council. London, March 1957. 53 p. (Research and Memoranda no. 3123)

5. Head, M. R. Approximate methods of calculating the two-dimensional laminar boundary layer with suction. In: G. V. Lachmann's Boundary layer and flow control. London. Pergamon Press, 1961. p. 801-841.

6. Howarth, L. On the calculation of steady flow in the boundary layer near the surface of a cylinder in a stream. Aeronautical Research Council 1:320-375. July 1957. (Research and Memoranda no. 1632)

7. International Business Machines Corporation. Reference manual 1620 Fortran. San Jose, California, 1962. 94 p.

8. Von Kármán, T. Über laminare und turbulente Reibung. Zeitschrift für angewandte Mathematik und Mechanik 1:233-251. 1921. (Translated in National Advisory Committee for Aeronautics (Technical Memoranda no. 1092). 1946.

9. Kuethe, A. M. and J. D. Schetzer. Foundations of aerodynamics. New York, Wiley, 1959. 446 p.

10. McCracken, Daniel D. A guide to Fortran programming. New York, Wiley, 1961. 88 p.

11. Pai, Shih-I. Viscous flow theory. vol 1. laminar flow. Princeton, New Jersey, 1956. 384 p.

12. Pohlhausen, K. Zur näherungsweisen Intergration der Differentialgleichung der laminare Grenzschicht. Zeitschrift für angewandte Mathematik und Mechanik 1:252-268. 1921.

13. Prandtl, L. and O. G. Tietjens. Fundamentals of hydro- and aeromechanics. New York, Dover, 1934. 270 p.

14. Rheinboldt, Werner. On the calculation of steady boundary layers for continuous suction with discontinuously variable suction velocity. Breisgau (Translated in National Aeronautics and Space Administration (Technical Translation. no. TT F-29). March 1957. 101 p.

15. Schlichting, H. Boundary layer theory. Karlsruhe, Verlag G. Braun, 1955. 535 p.

16. Witting, H. Verbesserung des Differenzenverfahrens von H. Görtler zur Berechnung laminarer Grenzschichten. Zeitschrift fur angewandte Mathematik und Physik 4:376-397. 1953.

APPENDICES

APPENDIX A

Derivation of the Momentum Integral Equation (quoted from Head (5, p. 802-805)

For steady two-dimensional incompressible flow the boundary layer equations are

$$u\frac{\partial u}{\partial x} + v\frac{\partial u}{\partial y} = -\frac{1}{\rho}\frac{dp}{dx} + \nu\frac{\partial^2 u}{\partial y^2} \qquad (1)$$

and

$$\frac{\partial u}{\partial x} + \frac{\partial v}{\partial y} = 0 \qquad (2)$$

The first of these two equations represents the Navier-Stokes equations when the boundary layer approximations are applied; the second is of course the continuity equation.

If we multiply (2) by u and add to (1), then we obtain

$$2u\frac{\partial u}{\partial x} + \frac{\partial}{\partial y}(uv) = U\frac{dU}{dx} + \nu\frac{\partial^2 u}{\partial y^2} \qquad (3)$$

where we have used Bernoulli's equation, applied outside the boundary layer, to substitute for $-(1/\rho)(dp/dx)$. We can write (3)

$$-\frac{\partial}{\partial x}(U^2 - u^2) + U\frac{dU}{dx} + \frac{\partial}{\partial y}(uv) = \nu\frac{\partial^2 u}{\partial y^2}$$

and, if we integrate over y through a distance h from the surface, where h is a distance greater than the boundary layer thickness we

obtain

$$-\int_o^h \frac{\partial}{\partial x}(U^2 - u^2)\,dy + \int_o^h U\frac{dU}{dx}\,dy + [\,uv\,]_o^h = \nu\left[\frac{\partial u}{\partial y}\right]_o^h \qquad (4)$$

Now, at

$$y = 0 \quad u = 0 \quad \frac{\partial u}{\partial y} = \frac{1}{\mu}\tau_o$$

and at

$$y = h \quad u = U \quad v = v_o + \int_o^h \frac{\partial v}{\partial y}\,dy \text{ and } \frac{\partial u}{\partial y} = 0$$

Also, $\partial v/\partial y = -\partial u/\partial x$ from (2), so that (4) may be written

$$-\int_o^h \frac{\partial}{\partial x}(U^2-u^2)\,dy + U\int_o^h \frac{\partial}{\partial x}(U-u)\,dy + Uv_o = -\frac{\tau_o}{\rho} \qquad (5)$$

Now, if h is constant independent of x we may write (5) as

$$-\frac{d}{dx}U^2\int_o^h\left[1 - \left(\frac{u}{U}\right)^2\right]dy + U\frac{d}{dx}U\int_o^h\left(1 - \frac{u}{U}\right)dy + Uv_o = \frac{\tau_o}{\rho} \qquad (6)$$

or

$$-\frac{d}{dx}U^2(\theta + \delta^*) + U\frac{d}{dx}U\delta^* + Uv_o = -\tau_o/\rho \qquad (7)$$

Differentiating out and rearranging we find that this becomes

$$\frac{d\theta}{dx} = \frac{\tau_o}{\rho U^2} - (H + 2)\frac{\theta}{U}\frac{dU}{dx} - \frac{v_s}{U}$$

Alternative derivation: We can obtain the foregoing momentum integral equation somewhat more directly by considering the flux of x-momentum through an elementary control volume of height h (greater than the boundary layer thickness) and length x (see Figure 17)

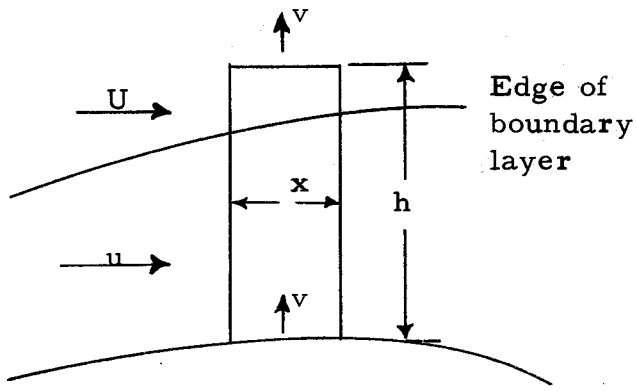

Figure 17. Sketch of the boundary layer

The nett efflux of x-momentum from the control volume per unit time is

$$\delta x \frac{d}{dx} \int_o^h \rho u^2 dy + \rho U v_h \delta x$$

and the nett force on the fluid in the x-direction is

$$-\tau_o \delta x - h \frac{dp}{dx} \delta x$$

Equating these expressions and substituting, as before, $U(dU/dx)$ for $-(1/\rho)(dp/dx)$ we obtain

$$\frac{d}{dx} \int_o^h u^2 dy + U v_h = -\frac{\tau_o}{\rho} + h U \frac{dU}{dx}$$

Since h is a constant independent of x we may write this

$$\frac{d}{dx} \int_o^h u^2 dy + U \left[v_o + \int_o^h \frac{\partial v}{\partial y} dy \right] = -\frac{\tau_o}{\rho} + U \frac{d}{dx} \int_o^h U \, dy$$

or

$$\frac{d}{dx} \int_o^h u^2 dy + U v_o - U \frac{d}{dx} \int_o^h u dy = -\frac{\tau_o}{\rho} + \frac{d}{dx} \int_o^h U^2 dy - U \frac{d}{dx} \int_o^h U \, dy$$

which gives

$$-\frac{d}{dx} U^2 \int_o^h \left[1 - \left(\frac{u}{U}\right)^2 \right] dy + U \frac{d}{dx} U \int_o^h \left(1 - \frac{u}{U}\right) dy + U v_o = - \frac{\tau_o}{\rho}$$

This equation is seen to be identical with (6) above and the same result follows.

APPENDIX B

Derivation of the Energy Integral Equation and the First Compatibility Condition at the Surface (quoted from Head (4, p. 24-25))

As before

$$u\frac{\partial u}{\partial x} + v\frac{\partial u}{\partial y} = U\frac{dU}{dx} + \nu\frac{\partial^2 u}{\partial y^2} \tag{1}$$

and

$$\frac{\partial u}{\partial x} + \frac{\partial v}{\partial y} = 0 \tag{2}$$

If we add $u/2\ (\partial u/\partial x + \partial v/\partial y)$ to the left hand side of (1), multiply through by u, and integrate from $y = 0$ to $y = h$, we have

$$\int_o^h \frac{3}{2}u^2\frac{\partial u}{\partial x}\,dy + \int_o^h uv\frac{\partial u}{\partial y}\,dy + \int_o^h \frac{1}{2}u^2\frac{\partial v}{\partial y}\,dy - U\int_o^h u\frac{dU}{dx}\,dy \tag{3}$$

$$= \nu\int_o^h u\frac{\partial^2 u}{\partial y^2}\,dy$$

<u>i.e.</u>,

$$\frac{d}{dx}\int_o^h \left(\frac{1}{2}u^3 - \frac{1}{2}uU^2\right)dy + \frac{1}{2}\int_o^h U^2\frac{\partial u}{\partial x}\,dy + \frac{1}{2}\left[u^2 v\right]_o^h$$

$$= \left[vu\frac{\partial u}{\partial y}\right]_o^h - \nu\int_o^h\left(\frac{\partial u}{\partial y}\right)^2 dy,$$

or

$$-\frac{d}{dx}\int_o^h \frac{1}{2}u\,(U^2 - u^2)\,dy + \frac{1}{2}U^2\int_o^h \frac{\partial u}{\partial x}\,dy + \frac{1}{2}U^2\left[\int_o^h \frac{\partial v}{\partial y}\,dy - v_s\right]$$

$$= -\nu\int_o^h\left(\frac{\partial u}{\partial y}\right)^2 dy$$

Hence $$\frac{1}{2}\frac{d}{dx}\left\{U^3\int_o^h \frac{u}{U}\left[1-\left(\frac{u}{U}\right)^2\right]dy\right\} + \frac{1}{2} v_s U^2 = \nu\int_o^h\left(\frac{\partial u}{\partial y}\right)^2 dy$$

or

$$\frac{d}{dx}(U_\epsilon^3) = 2\nu\int_o^h\left(\frac{\partial u}{\partial y}\right)^2 dy - v_s U^2 \qquad (4)$$

where ϵ, the energy thickness,

$$= \int_o^h \frac{u}{U}\left[1-\left(\frac{u}{U}\right)^2\right] dy$$

This is the energy equation in its usual form

Now

$$\frac{d}{dx}\left(\frac{\epsilon}{\theta}\right) = \frac{1}{\theta}\frac{d\epsilon}{dx} - \frac{\epsilon}{\theta^2}\frac{d\theta}{dx}$$

so that

$$\frac{d\epsilon}{dx} = \theta\frac{dH_\epsilon}{dx} + H_\epsilon\frac{d\theta}{dx} \qquad (5)$$

where

$$H_\epsilon = \epsilon/\theta$$

Also

$$\frac{d}{dx}(U^3\epsilon) = 3U^2\epsilon\frac{dU}{dx} + U^3\frac{d\epsilon}{dx}$$

which from (5) becomes

$$\frac{d}{dx}(U^3\epsilon) = 3U^2\epsilon\frac{dU}{dx} + U^3\theta\frac{dH_\epsilon}{dx} + U^3 H_\epsilon\frac{d\theta}{dx}$$

Substituting for $d/dx\ (U^3\epsilon)$ in (4) we have

$$3U^2\epsilon\frac{dU}{dx} + U^3\theta\frac{dH\epsilon}{dx} + U^3 H\epsilon\frac{d\theta}{dx} + v_s U^2 = 2\nu\int_o^h\left(\frac{\partial u}{\partial y}\right)^2 dy$$

Substituting for $d\theta/dx$ from (3) and re-arranging, we find

$$\frac{U\theta^2}{\nu}\frac{dH\epsilon}{dx} = \frac{2\theta}{U^2}\int_o^h\left(\frac{\partial u}{\partial y}\right)^2 dy - H\epsilon\left[\frac{\theta}{U}\left(\frac{\partial u}{\partial y}\right)_o - (H-1)\frac{\theta^2}{\nu}\frac{dU}{dx} - \frac{v_s\theta}{\nu}\right] - \frac{v_s\theta}{\nu}$$

which may be re-written

$$H\epsilon' = \frac{1}{\overline{U}t^*}\left[2D^* - H\epsilon\left\{\ell - \Lambda(H-1) - \lambda\right\} - \lambda\right]$$

where

$$D^* = \int_o^{h/\theta}\left(\frac{\theta}{U}\right)^2\left(\frac{\partial u}{\partial y}\right)^2 d\left(\frac{y}{\theta}\right)$$

and the other symbols are as defined above, the prime denoting as before differentiation with respect to $\overline{x}$ ($\overline{x} = x/c$).

Boundary Layer Equation at the Surface

At the surface, $v = -v_s$, $u = 0$ and $\partial u/\partial x = 0$. Hence the boundary layer equation for two-dimensional incompressible flow becomes

$$-v_s\left(\frac{\partial u}{\partial y}\right)_o = U\frac{dU}{dx} + \nu\left(\frac{\partial^2 u}{\partial y^2}\right)_o ,$$

where the subscript o refers, as elsewhere, to conditions at the surface. Multiplying through by $\theta^2/U\nu$ this becomes

$$-\frac{v_s\theta}{\nu}\frac{\theta}{U}\left(\frac{\partial u}{\partial y}\right)_o = \frac{\theta^2}{\nu}\frac{dU}{dx} + \frac{\theta^2}{U}\left(\frac{\partial^2 u}{\partial y^2}\right)_o$$

which may be written

$$-\lambda \ell = \Lambda + m$$

or

$$m = -(\Lambda + \ell \lambda)$$

where

$$m = \frac{\theta^2}{U} \left(\frac{\partial^2 u}{\partial y^2} \right)_o$$

(The boundary layer equation at the surface is referred to as the first compatibility at the surface)

APPENDIX C

Derivation of the Potential Flow Distribution About a Circular Cylinder With Lift

The velocity in the ϕ direction for circulatory flow about a cylinder in a uniform stream is given by the expression

$$U = Uo \sin(\phi)\left(1 + \frac{a}{r}\right) + \frac{\Gamma}{2\pi r} \qquad (9, \text{ p. } 66)$$

The flow along the surface of a cylinder of radius "a" is

$$U = Uo \sin(\phi)\ 2 + \frac{\Gamma}{2\pi a}$$

at $\phi = \phi_s$, $U = 0$, therefore

$$0 = Uo\ 2 \sin(\phi_s) + \frac{\Gamma}{2\pi a}$$

$$-2\ Uo \sin(\phi_s) = \frac{\Gamma}{2\pi a}$$

therefore

$$U = 2\ Uo \sin(\phi) - 2\ Uo \sin(\phi_s)$$

or

$$\frac{U}{Uo} = 2(\sin(\phi) = \sin(\phi_s)) \qquad (1)$$

For positive lift ϕ_s will be greater than π, and sin (ϕ_s) will be negative. Equation (1) above is an expression for the velocity distribution $(\overline{U})$ along the surface of the cylinder which appears in the momentum and energy integral relations. Also required is the velocity gradient which is obtained from equation (1).

$$\frac{d(U/Uo)}{d(x/c)} = \frac{d\ (2\ (\sin\phi - \sin\phi_s)\ )}{d\,(x/c)}$$

$$\frac{d\,\overline{U}}{d\,\overline{x}} = 4\cos\ \phi \qquad (2)$$

since $\phi = 2\,(x/c)$ and $\frac{d\ (\phi)}{d\,(x/c)} = 2$. Equation (2) is used to evaluate the term Λ which appears in the first compatibility condition as well as the momentum and energy integral relations.

$$\Lambda = t^* \frac{d\overline{U}}{d\,\overline{x}}$$

or

$$\Lambda = t^*\ 4\cos\ \phi \qquad (3)$$

APPENDIX D

Derivation of the Suction Distribution for a Uniform Porosity Cylinder

The suction distribution is assumed to be that from a cylinder of uniform porosity, where the distribution of suction is the result of the potential pressure distribution on the outside of the cylinder, and the pressure within the cylinder is uniform. Note that this potential pressure distribution is valid only in the absence of separation.

Assume that the value of v_s, the suction velocity, is given by the expression

$$v_s = K\sqrt{(P - P_1)} \tag{1}$$

where

K is a constant indicating the resistance of the surface to the inflow of air.

P is the pressure on the outside of the boundary layer.

P_1 is the uniform pressure inside the cylinder.

Bernouli's equation can be applied to relate P to the velocity at the outside edge of the boundary layer.

$$P = Po + \frac{1}{2}\rho\, Uo^2 - \frac{1}{2}\rho\, U^2$$

where

Po is the pressure of the free stream.

We have already assumed that the velocity at the outside edge of the boundary layer is given by the potential flow about a circular cylinder (see Appendix C). Using this information we obtain

$$P = Po + \frac{1}{2}\rho\, Uo^2 - \frac{1}{2}\rho\,(\,2Uo\,(\sin(\phi) - \sin(\phi_s)\,)^{\,2} \qquad (2)$$

subtracting P_1 from equation (2) yields

$$P - P_1 = (Po + \frac{1}{2}\,\rho\, Uo^2 - P_1) - 2\,Uo\,\rho\,(\sin(\phi) - \sin(\phi_s))^{\,2}$$

Using equation (1)

$$v_s = K\sqrt{(Po + \frac{1}{2}\,\rho\, Uo - P_1) - 2\rho\, Uo\,(\sin(\phi) - \sin(\phi_s)\,)^{\,2}} \qquad (3)$$

v_s^* can be found from v_s^* by the following expression

$$v_s^* = \frac{v_s}{Uo}\sqrt{\frac{Uo\ c}{\nu}}$$

Using v_s from equation (3) in the above expression yields

$$v_s^* = \sqrt{\frac{(K)}{Uo}(Po + \frac{1}{2}\rho\, Uo - P_1)\frac{(Uo\,c)}{\nu} - (2\,\rho\, Uo)\frac{(K)}{Uo}\,\frac{(Uo\,c)}{\nu}(\sin(\phi) - \sin(\phi_s)\,)^2}$$

This expression can be put in the form

$$v_s^* = \sqrt{A - B\,(\sin(\phi) - \sin(\phi_s)\,)^2} \qquad (4)$$

where A and B are constants.

APPENDIX E

Fortran Programs Used With Explanation and Flow Diagram

Section V discussed adapting Head's method to the digital computer. In this appendix the program is shown, along with a flow diagram and an explanation of some of the program details. The machine used was an IBM 1620 with 40,000 units of core storage which is under the supervision of the Statistics Department of Oregon State University. Fortran I was the compiler language incorporated.

The program was complicated by the fact that difficulty was encountered in getting it and the large table into the memory of the machine without an "overlap" condition. It was found necessary to break the tables into two parts, and then include only two of the three types of suction distribution with each part. This results in four programs: two for the upper part of the table and two for the lower part of the table. Shown is the program for the upper part of the table with the uniform porosity cylinder suction distribution and Ando's suction distribution (see Section VI). Following this program are the statements which are necessary to modify the program for the lower half of the table. These statements are to be inserted in the locations of corresponding hand written numbers. The mark (X) indicates those statements in the program which are to be removed in modifying for

the lower half of the table. Not included at all are the statements to adapt the program to Rheinboldt's suction distribution. The Rheinboldt program is essentially the same, except for the change in suction distribution. The suction distribution in the program shown is chosen by assigning the value (1) or (2) to the fixed point variable J1 through an input card (See statement following statement (49), and see statement (17)).

Two explanations are of greatest significance in following the program. They are the correspondence between the values in the tables and Figures 21, 22, and 23, and the correspondence between the variables which appear in the program and the variables which are used in the text of this thesis.

Consider first Figure 21. As mentioned in Section V the table for this figure is in the form $m = m(\ell, H_\epsilon)$. Since a floating point variable is desired for the table the double subscripted variable A has been used to represent m. The range of m in Figure 21 covers the values $H_\epsilon = 1.50$ to $H_\epsilon = 1.76$ in increments of 0.01. These same increments were chosen for the table so that subscript (1) corresponds to $H_\epsilon = 1.50$ and subscript (27) corresponds to $H_\epsilon = 1.76$. As was mentioned, the table had to be divided. The parameter ℓ extends from the value $\ell = 0.0$ to $\ell = 0.6$. This was divided into two parts: high friction profiles, $\ell = 0.2$ to $\ell = 0.6$ and low friction

profiles, $\ell = 0.0$ to $\ell = 0.4$. On the upper part of the table subscript (1) corresponds to $\ell = 0.2$ and subscript (21) corresponds to $\ell = 0.6$. On the lower part of the table subscript (1) corresponds to $\ell = 0.0$ and subscript (21) corresponds to $\ell = 0.4$.

The tables for Figures 22 and 23 are very similar to one another. As mentioned earlier they are of the form $H(\ell, m)$ and $2D^*(\ell, m)$ respectively. The corresponding double subscripted variables in the program are H and D. The subscripts which correspond to ℓ are the same as in the first table. The parameter m extends from the value $m = -0.5$ to $m = +0.2$. The corresponding subscripts are (1) for $m = -0.5$ and (21) for $m = +0.2$. In the program subscripts L and M correspond to the parameters ℓ and m. The subscript I (not in the "DO" loop) is used to represent H_ϵ.

It will be noticed from Figures 21, 22, and we that with the choice of subscripts just discussed large areas of the table are blank, that is, data is not given in Figures 21, 22, and 23 for all of the locations set aside in the memory of the machine for the tables. Some of these blank table locations are used as variables in the equations as will be explained. All of the other blank locations have been assigned the number (9.000), and it can be seen in the program that before a value from the table is ever used it is first checked that it does not have the value (9.000), which can only mean that the calculation has

gone off the figure. If a (9.000) is discovered the words "OFF CHART" are printed and the machine stops.

As just mentioned some of the otherwise unused table values have been used as variables which appear in the equations. Figures 22 and 23 have the region $\ell = 0.0$ to $\ell = 0.2$ and $m = -0.5$ to $m = -0.3$ in this blank category. Given in this section is a key to relate the variables which appear in the program with the variables which appear in the text of the thesis.

Other items which might assist one in following the program are the value of the fixed point variable J (following statement (34)). Using the symbols introduced in Section V $J = 1$ when the value of ℓ_a is being found, and $J = 2$ when the value of ℓ_b is being found. On page 30 of Section V the statement is made, "To find a assume that the algebraic value of the slope of the line d-d is greater than the algebraic value of the slope of $H_{\epsilon 2}$ near the point of intersection". This slope is checked at statement (79). If the slopes are found to be equal the machine prints "IMPROPER SLOPES" and stops. If the slopes are reversed the machine prints, "IMPROPER SLOPES", reverses the correction for the new choice of ℓ, then continues to calculate. If, however, Head's method has broken down and the two lines do not intersect then the machine gets caught in a loop, that is, the corrections for a new choice of ℓ will oscillate from left to right

on Figure 21, and the machine will indefinitely "hunt" for an intersection which does not exist. When this occurs the machine, after twenty new choices of ℓ, will print "EXCESSIVE LOOPS" and stop. This is done through the fixed point variable N (following statement (20)). Statements (23) to (34) are for Lagrange interpolation used with Ando's suction distribution. The final item which I will discuss concerning the mechanics of the program is the use of the sense switches (program switches). All four are used. Switch 1 sets the increment along the surface of the cylinder at which calculations are made at one degree. Switch 2 sets this increment at one-third of a degree. Switch 3 engages the console typewriter for observation of results in addition to the punch card output. This is used in deciding on the settings of switches 1, 2, and 4. Switch 4 causes the machine to stop. If it can be seen that the results are going erratic or it is found otherwise desirable to stop the calculation this last switch can be used.

The running time for this program on the 1620 was about seven and one-half loops per minute, where a loop consists of all the calculations at one position on the airfoil. This time is increased when Sense Switch 3 is "on" because of the relatively slow typewriter output.

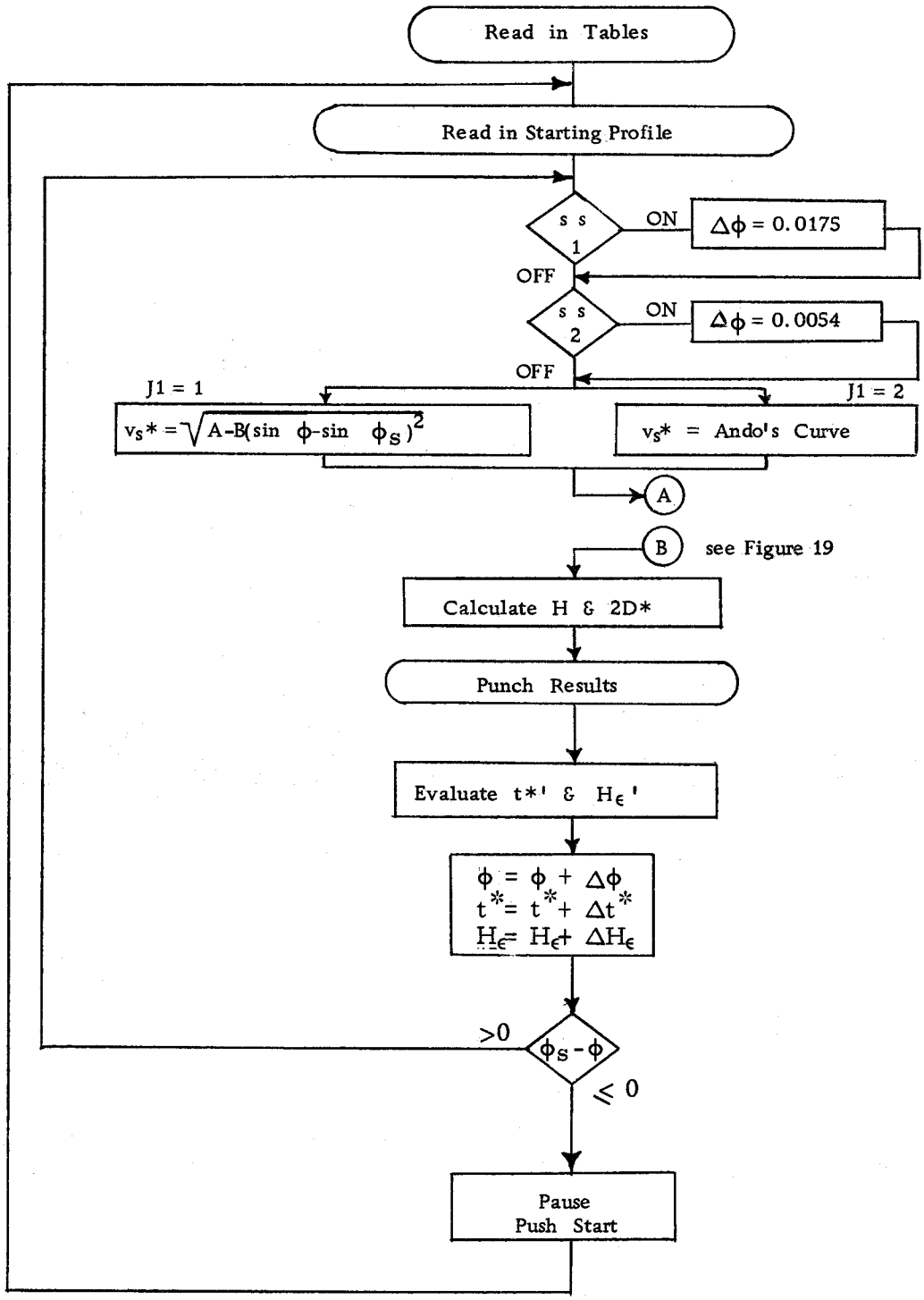

Figure 18. Flow diagram for Fortran program.

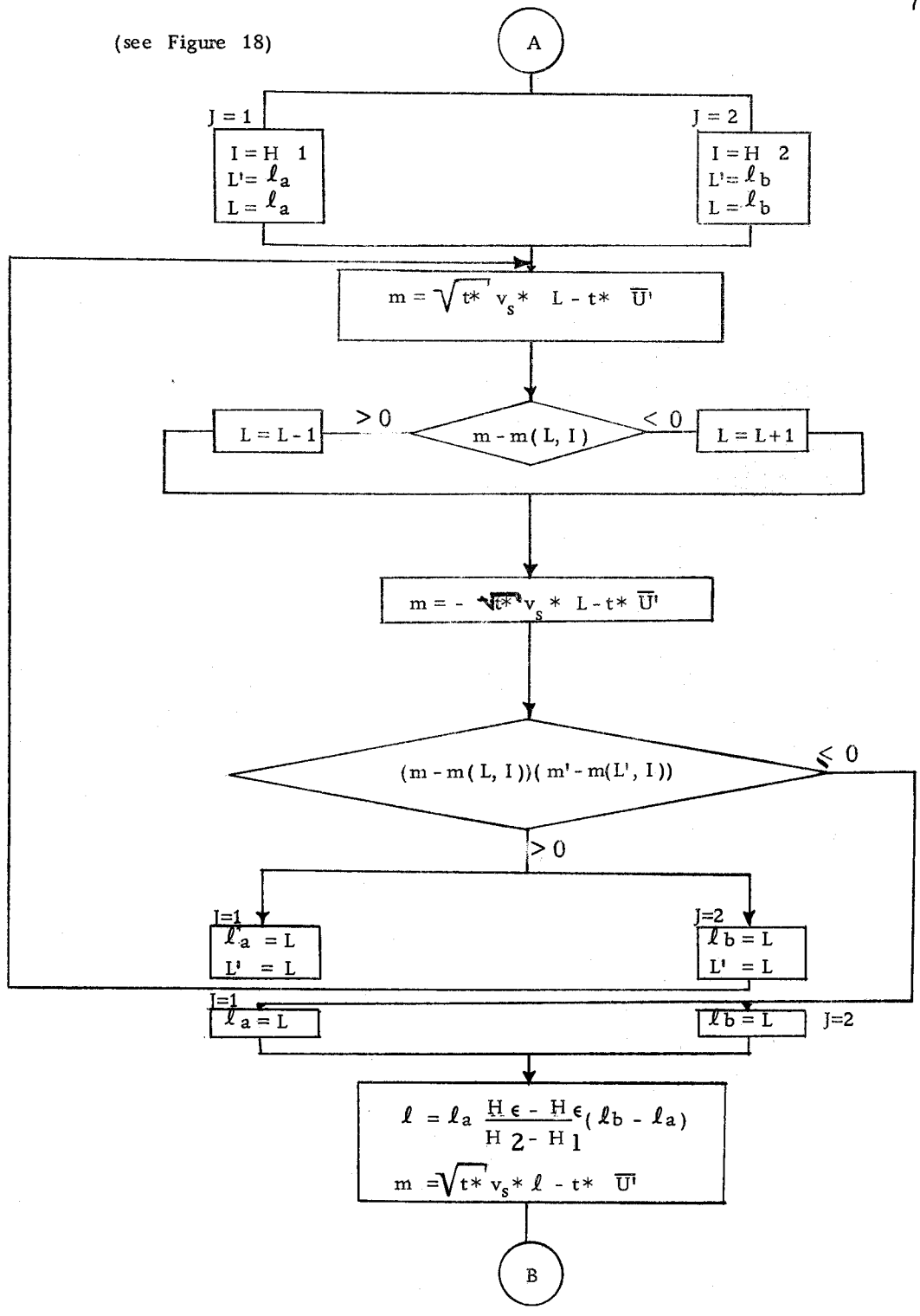

Figure 19. Flow diagram for Fortran program to find the intersection on the H chart.

Table 1. Correspondence between variables used in the program and variables which appear in the text of the thesis.

H(1,1) - H interpolated
H(1,4) - ℓ_i
H(1,5) - m_i
H(2,1) - ℓ_{ai}
H(2,2) - ℓ_{bi}
H(2,3) - $H_{\epsilon 2}$
H(2,4) - $H_{\epsilon 3}$
H(2,5) - V_s^*
H(3,1) - m at ℓ_a
H(3,2) - m at ℓ_b
H(3,3) - $\Delta\ell$ = 0.020
H(3,4) - Δm= 0.033
H(3,5) - $\Delta\phi$
H(4,1) - ℓ_a
H(4,2) - ℓ_b
H(4,3) - $(dt^*/d\bar{x})$ $(\Delta\phi)$
H(4,4) - $(dH/d\bar{x})$ $(\Delta\phi)$
H(4,5) - t^*
H(5,1) - H_ϵ
H(5,2) - ϕ (K-1)
H(5,3) - ϕ (K)
H(5,4) - ϕ (K+1)
H(5,5) - ϕ (K+2)

D(1,1) - $2D^*$ interpolated
D(1,2) - W Rheinboldt suction distribution
D(1,3) - Z " " "
D(1,4) - Y " " "
D(1,5) - A Uniform Porosity Cylinder suction distribution
D(2,1) - B " " " " "
D(2,2) - ϕ_s
D(2,3) - sin ϕ_s
D(2,4) - ϕ
D(2,5) - ℓ
D(3,1) - m
D(5,4) - temporary storage (see statement (75))
D(5,5) - temporary storage (see statement (28))

Table 2. Fortran program for the uniform porosity cylinder and the part of the table giving modification for the lower part of the table.

```
      DIMENSION H (21, 21),  D (21, 21),  A (21, 27), V( 19)
      DO  50  I = 1, 21
      DO  51  J = 1, 15, 7
    READ 1,  H (I, J), H(I, J+1), H(I, J+2), H(I, J+3), H(I, J+4), H(I, J+5), H(I, J+6)
    READ 1,  D (I, J), D(I, J+1), D(I, J+2), D(I, J+3), D(I, J+4), D(I, J+5), D(I, J+6)
51  READ 1,  A (I, J), A(I, J+1), A(I, J+2), A(I, J+3), A(I, J+4), A(I, J+5), A(I, J+6)
50  READ 8,  A (I, 22), A(I, 23), A(I, 24), A(I, 25),  A(I, 26),  A(I, 27)
      DO  52  I = 1, 8, 7
52  READ 1,  V(I), V(I+1), V(I+2), V(I+3), V(I+4), V(I+5), V(I+6)
    READ 9,  V(15), V(16), V(17), V(18), V(19)
49  READ 10, H(4, 5), H(5, 1), D(2, 4), H(3, 5), D(2, 2), D(2, 3), H(2, 1), H(2, 2)
    READ 86, D(1, 5), D(2, 1), J1
42  IF (SENSE SWITCH 1) 11,  12
11  H(3, 5) = 0. 0174533
12  IF (SENSE SWITCH 2) 13,  16
13  H(3, 5) = 0. 0053599
16  IF (SENSE SWITCH 4) 48,  17
17  GO  TO (70, 72),  J1
70  IF (D (2, 4) -1. 570796)40, 41, 41
40  H (2, 5) = 0.
    GO  TO  34
41  H (2, 5) = SQRTF (D (1, 5) - D(2, 1)*(SINF (D (2, 4) ) - D(2, 3) ) ** 2)

    GO  TO  34
72  IF (D (2, 4) - 1. 570796) 29, 23, 23
29  H (2, 5) = 0.
    GO  TO  34
23  K = (D(2, 4) - 1. 570796)* 18. 0/3. 1415927 + 1. 0
    IF (K - 17) 74,  73,  73
73  K = 17
74  IF (2 - K) 75,  76,  76
76  K = 2
75  H (5,  2) = K - 2
    H (5,  2) = (H(5, 2)*3. 1415927/18. ) + 1. 5707963
    H (5,  3) = K - 1
    H (5,  3) = (H(5, 3)*3. 1415927/18. ) + 1. 5707963
    H (5,  4) = K
    H (5,  4) = (H(5, 4)*3. 1415927/18. 0) + 1. 5707963
    H (5,  5) = K + 1
    H (5,  5) = (H(5, 5)*3. 1415927/18. 0) + 1. 5707963
    H (2,  5) = (H(5, 3) - D(2, 4))*(H(5, 4) - D (2, 4) )*(H(5, 5) -D (2, 4) )*V(K -1)
    H (2,  5) = H(2,  5)/((H(5, 3) -H (5, 2))*(H(5, 4) -H(5, 2))*(H(5, 5) -H(5, 2)))
    D (5,  4) =  (H(5, 2) - D(2, 4) )*(H(5, 4) - D(2, 4))*(H(5, 5) -D(2, 4) )*V(K)
    D (5,  4) = D(5, 4)/((H(5, 2) -H(5, 3) )*(H(5, 4) -H(5, 3) )*(H(5, 5) -H(5, 3) ))
    H (2,  5) = H(2, 5) + D (5, 4)
    D (5,  4) =  (H(5, 2)-D(2, 4))*(H(5, 3) - D(2, 4))*(H(5, 5) - D(2, 4))* V(K+1)
    D (5,  4)= D(5, 4)/((H(5, 2) - H(5, 4))*(H(5, 3) - H (5, 4))*(H(5, 5) - H (5, 4)))
    H (2,  5) = H(2, 5) + D(5, 4)
```

```
      D (5, 4) =  (H(5, 2) - D(2, 4))*H(5, 3) - D(2, 4))*(H(5, 4) - D(2, 4))* V(K+2)
      D (5, 4) = D(5, 4)/((H(5, 2) - H(5, 5))*(H(5, 3)-H(5, 5))*(H(5, 4) - H(5, 5)))
      H (2, 5) = H(2, 5) + D(5, 4)
   34 I = (H(5, 1) - 1.5)*100. + 1.
      J = 1
   31 D (2, 5) = H (2, J)
1  X  L = 50. * (H(2, J) - 0.2)+1.
      D(3, 1) = - SQRTF (H(4, 5))*H(2, 5)* D(2, 5) - H( 4, 5)* 4. * COSF (D(2, 4))
      N = 1
   30 IF ( A( L + 1, I ) - 9. ) 78, 61, 78
   78 IF (A( L, I ) - 9. ) 79, 61, 79
   79 IF((A(L + 1, I) - A(L, I))/H(3, 3) + SQRTF (H(4, 5))*H(2, 5)) 21, 22, 33
   33 H ( 3, J ) = D ( 3, 1)
      PRINT 6
      PUNCH 6
      IF ( D(3, 1) - A(L, I)) 26, 25, 24
   21 H(3, J) = D(3, 1)
      IF (D(3, 1) - A(L, I)) 24, 25, 26
   24 L = L + 1
      GO TO 27
   26 L = L - 1
   27 D( 2, 5) = L - 1
2  X  D ( 2, 5) = D(2, 5)/50. + 0.2
      D( 3, 1) = -SQRTF ( H (4, 5))*H (2, 5)* D (2, 5) -H (4, 5)* 4. * COSF(D(2, 4))
3  X  IF(D(2, 5) - 0.6 ) 77, 61, 61
4  X77 IF(D(2, 5) - 0.2 ) 38, 20, 20
   X38 PRINT 10, H(4, 5), H(5, 1), D(2, 4), H(3, 5), D(2, 2), D(2, 3), H(2, 1), H(2, 2)
   X   PUNCH 10, H(4, 5), H(5, 1), D(2, 4), H(3, 5), D(2, 2), D(2, 3), H(2, 1), H(2, 2)
   X   PRINT 86, D(1, 5), D(2, 1), J1
   X   PUNCH 86, D(1, 5), D(2, 1), J1
   X   GO TO 48
5  X20 L1 = 50. *(H(2, J) - 0.2 ) + 1.
      N = N + 1
      IF(20 - N) 45, 45, 18
   18 IF(A(L, I) - 9.) 35, 61, 35
   35 IF(( A(L, I) - D(3, 1))*(A(L1, I) -H (3, J))) 28, 25, 80
   80 H(2, J) = D(2, 5)
      GO TO 30
   28 H(4, J) = A(L, I)*H(2, J) - A (L1, I)* D(2, 5)
      H(4, J) = H(4, J ) + H(4, 5)* 4. * COSF (D(2, 4))*(H(2, J) - D(2, 5))
      H(5, 5)= -SQRTF(H(4, 5))*H(2, 5)*(H(2, J) - D(2, 5)) - A(L1, I) + A (L, I)
      H(4, J) = H(4, J)/H(5, 5)
      H(2, J) = D(2, 5)
   25 I = I + 1
      J = J + 1
      IF(J - 3 ) 31, 32, 32
   32 H(2, 3) = I - 3
      H(2, 4) = I - 2
      H(2, 3) =( H(2, 3) + 150. )/100.
      H(2, 4) =(H (2, 4) + 150. )/100.
D(2, 5) = (H(4, 2)*(H(5, 1)-H(2, 3))+H(4, 1)*(H(2, 4)-H(5, 1)))/(H(2, 4)-H(2, 3))
D(3, 1) = -SQRTF(H(4, 5))*H(2, 5)* D(2, 5) -H(4, 5)* 4. * COSF(D(2, 4))
```

```
      IF(D(3,1) + 0.50) 61, 61, 36
   36 IF(0.1666666667 - D(3,1)) 61, 61, 37
   37 M=D(3,1)* 30. + 16.
6  X  L = 50. *( D(2,5) - 0.2) + 1.
      H  (1,4) = L -1
7  X  H  (1,4) = H(1,4)/50. + 0.2
      H  (1,5) = M
      H  (1,5) = (H(1,5) - 16.)/30.
      IF  (H(L,M) - 9.) 62, 61, 62
   62 IF  (H(L + 1, M) - 9.) 63, 61, 63
   63 IF  (H(L,M + 1) - 9.) 64, 61, 64
   64 H  (1,1) = H(L,M) + (H(L + 1,M) - H(L,M))*(D(2,5) - H(1,4))/H(3,3)
      H  (1,1) = H(1, 1) + (H(L,M + 1) - H(L,M))*(D(3,1) - H(1,5))/H(3,4)
      IF  (D(L,M) - 9.) 65, 61, 65
   65 IF  (D(L + 1,M)-9.) 66, 61, 66
   66 IF  (D(L,M + 1) - 9.) 67, 61, 67
   67 D  (1,1) = D(L,M) + (D(L + 1,M) - D(L,M))*(D(2,5) - H(1,4))/H(3,3)
      D  (1,1) = D(1, 1) + (D(L, M+1) - D(L, M))*(D(3,1) - H(1,5))/H(3,4)
      IF  (SENSE SWITCH 3) 15, 14
   15 PRINT 5, D(2,4), H(2,5), H(4,5), H(5,1), D(3,1), D(2,5), D(1,1), H(1,1)
   14 PUNCH 5,D(2,4), H(2,5), H(4,5), H(5,1), D(3,1), D(2,5), D(1,1), H(1,1)
H(4,3) = D(2,5)-H(4,5)*4. *COSF(D(2,4))*(H(1,1)+2.) - SQRTF(H(4,5))*H(2,5)
      H(4,3) = H(3,5)*H(4,3)/(SINF(D(2,4)) -D(2,3))
H(4,4) = D(2,5)-H(4,5)*4. *COSF(D(2,4))*(H(1,1)-1.)-SQRTF(H(4,5))*H(2,5)
      H(4,4) =H(3,5)* (D(1,1) -H(5,1)*H(4,4) - SQRTF(H(4,5))*H(2,5))
      H(4,4) =H(4,4)/ (2. *H(4,5)*( SINF(D(2,4)) - D(2,3)))
      D(2,4) = D(2,4) + H(3,5)
      H(4,5) = H(4,5) + H(4,3)/2.
      H(5,1) = H(5,1) + H(4,4)/2.
      IF(D(2,2)-D(2,4)) 48, 48, 42
   48 PAUSE
      GO TO 49
   22 PRINT 6
      PUNCH 6
      GO TO 48
   61 PRINT 7
      PUNCH 7
      GO TO 48
   45 PRINT 85
      PUNCH 85
      GO TO 48
    1 FORMAT(7F6.3)
    5 FORMAT(8F8.4)
    6 FORMAT(15HIMPROPER SLOPES)
    7 FORMAT(9HOFF CHART)
    8 FORMAT(6F6.3)
    9 FORMAT(5F6.3)
   10 FORMAT(8F7.4)
   85 FORMAT(15HEXCESSIVE LOOPS)
   86 FORMAT(2F8.4,I2)
      END
```

```
1          L = 50. * H (2, J) + 1.
2          D (2, 5) = D (2, 5) / 50.
3          IF (D(2, 5) - 0.4) 77, 61, 61
4     77   IF (D(2, 5)) 48, 20, 20
5     20   L1 = (H(2, J))* 50. + 1.
6          L = 50. * D (2, 5) + 1.
7          H (1, 4) = H (1, 4)/50.
```

APPENDIX F

Computed Results

Table 3. Computed results for the solid boundary problem (ϕ = 180 degrees, $v_s^* = 0$)

ϕ	v_s^*	t^*	H_ϵ	m	ℓ	H
.3490	.0000	.0217	1.6300	-.0815	.3530	2.2383
.3491	.0000	.0217	1.6300	-.0815	.3531	2.2382
.3492	.0000	.0217	1.6300	-.0815	.3531	2.2380
.3493	.0000	.0217	1.6301	-.0815	.3532	2.2379
.3494	.0000	.0217	1.6301	-.0815	.3532	2.2377
.3495	.0000	.0217	1.6301	-.0815	.3533	2.2376
.3496	.0000	.0217	1.6302	-.0815	.3533	2.2374
.3497	.0000	.0217	1.6302	-.0815	.3534	2.2373
.3498	.0000	.0217	1.6302	-.0815	.3534	2.2371
.3499	.0000	.0217	1.6302	-.0815	.3535	2.2370
.3500	.0000	.0217	1.6303	-.0815	.3535	2.2369
.3501	.0000	.0217	1.6303	-.0815	.3536	2.2367
.3502	.0000	.0217	1.6303	-.0815	.3536	2.2366
.3503	.0000	.0217	1.6304	-.0815	.3537	2.2364
.3504	.0000	.0217	1.6304	-.0815	.3537	2.2363
.3505	.0000	.0217	1.6304	-.0815	.3538	2.2362
.3506	.0000	.0217	1.6305	-.0815	.3538	2.2360
.3507	.0000	.0217	1.6305	-.0815	.3539	2.2359
.3508	.0000	.0217	1.6305	-.0815	.3539	2.2357
.3509	.0000	.0217	1.6306	-.0815	.3540	2.2356
.3510	.0000	.0217	1.6306	-.0815	.3540	2.2355
.3511	.0000	.0217	1.6306	-.0815	.3541	2.2353
.3512	.0000	.0217	1.6307	-.0815	.3541	2.2352
.3513	.0000	.0217	1.6307	-.0815	.3541	2.2351
.3514	.0000	.0217	1.6307	-.0816	.3542	2.2349
.3515	.0000	.0217	1.6307	-.0816	.3542	2.2348
.3516	.0000	.0217	1.6308	-.0816	.3543	2.2347
.3517	.0000	.0217	1.6308	-.0816	.3543	2.2346
.3518	.0000	.0217	1.6308	-.0816	.3544	2.2344
.3519	.0000	.0217	1.6309	-.0816	.3544	2.2343
.3520	.0000	.0217	1.6309	-.0816	.3544	2.2342
.3521	.0000	.0217	1.6309	-.0816	.3545	2.2341
.3522	.0000	.0217	1.6309	-.0816	.3545	2.2339
.3575	.0000	.0218	1.6324	-.0817	.3568	2.2273
.3629	.0000	.0218	1.6334	-.0818	.3583	2.2229
.3682	.0000	.0219	1.6341	-.0820	.3594	2.2199
.3736	.0000	.0220	1.6345	-.0822	.3602	2.2176
.3789	.0000	.0221	1.6351	-.0824	.3611	2.2147
.3843	.0000	.0222	1.6355	-.0826	.3618	2.2126
.3897	.0000	.0223	1.6357	-.0828	.3623	2.2109
.3950	.0000	.0224	1.6360	-.0829	.3627	2.2096
.4004	.0000	.0225	1.6362	-.0831	.3631	2.2085
.4057	.0000	.0226	1.6363	-.0832	.3634	2.2076
.4111	.0000	.0227	1.6365	-.0834	.3637	2.2068
.4165	.0000	.0228	1.6366	-.0835	.3639	2.2061

Table 3 (Continued)

ϕ	v_s^*	t^*	H_ϵ	m	ℓ	H
.4218	.0000	.0229	1.6367	-.0836	.3641	2.2055
.4272	.0000	.0230	1.6368	-.0837	.3643	2.2050
.4325	.0000	.0230	1.6368	-.0838	.3645	2.2046
.4379	.0000	.0231	1.6369	-.0838	.3646	2.2042
.4433	.0000	.0232	1.6370	-.0839	.3647	2.2038
.4486	.0000	.0233	1.6370	-.0840	.3648	2.2035
.4540	.0000	.0233	1.6371	-.0840	.3649	2.2033
.4593	.0000	.0234	1.6371	-.0840	.3650	2.2030
.4647	.0000	.0235	1.6371	-.0841	.3650	2.2028
.4701	.0000	.0235	1.6372	-.0841	.3651	2.2027
.4754	.0000	.0236	1.6372	-.0841	.3651	2.2025
.4808	.0000	.0237	1.6372	-.0841	.3652	2.2024
.4861	.0000	.0237	1.6372	-.0841	.3652	2.2024
.4915	.0000	.0238	1.6372	-.0841	.3652	2.2023
.4969	.0000	.0239	1.6372	-.0841	.3652	2.2023
.5022	.0000	.0239	1.6373	-.0841	.3652	2.2022
.5076	.0000	.0240	1.6373	-.0841	.3652	2.2022
.5250	.0000	.0242	1.6373	-.0840	.3652	2.2023
.5425	.0000	.0244	1.6372	-.0838	.3650	2.2026
.5599	.0000	.0246	1.6372	-.0836	.3649	2.2030
.5774	.0000	.0249	1.6371	-.0834	.3646	2.2036
.5949	.0000	.0251	1.6370	-.0832	.3643	2.2043
.6123	.0000	.0253	1.6369	-.0829	.3640	2.2051
.6298	.0000	.0255	1.6367	-.0827	.3637	2.2059
.6472	.0000	.0258	1.6366	-.0823	.3633	2.2069
.6647	.0000	.0260	1.6364	-.0820	.3629	2.2080
.6821	.0000	.0263	1.6363	-.0816	.3624	2.2091
.6996	.0000	.0265	1.6361	-.0813	.3619	2.2103
.7170	.0000	.0268	1.6359	-.0809	.3614	2.2116
.7345	.0000	.0271	1.6357	-.0804	.3609	2.2130
.7519	.0000	.0273	1.6355	-.0800	.3603	2.2144
.7694	.0000	.0276	1.6352	-.0795	.3597	2.2158
.7868	.0000	.0279	1.6347	-.0790	.3587	2.2183
.8043	.0000	.0283	1.6343	-.0785	.3578	2.2204
.8217	.0000	.0286	1.6339	-.0779	.3570	2.2222
.8392	.0000	.0289	1.6336	-.0773	.3561	2.2240
.8567	.0000	.0293	1.6333	-.0767	.3553	2.2258
.8741	.0000	.0296	1.6329	-.0761	.3544	2.2276
.8916	.0000	.0300	1.6326	-.0754	.3535	2.2294
.9090	.0000	.0304	1.6322	-.0747	.3526	2.2313
.9265	.0000	.0308	1.6318	-.0740	.3517	2.2333
.9439	.0000	.0312	1.6315	-.0732	.3507	2.2354
.9614	.0000	.0316	1.6311	-.0725	.3497	2.2375
.9788	.0000	.0321	1.6306	-.0716	.3486	2.2397
.9963	.0000	.0325	1.6302	-.0708	.3475	2.2421

Table 3 (Continued)

ϕ	v_s^*	t^*	H_ϵ	m	ℓ	H
1.0137	.0000	.0330	1.6298	-.0699	.3463	2.2445
1.0312	.0000	.0335	1.6293	-.0690	.3451	2.2471
1.0486	.0000	.0341	1.6288	-.0680	.3438	2.2498
1.0661	.0000	.0346	1.6283	-.0670	.3424	2.2526
1.0835	.0000	.0352	1.6278	-.0659	.3410	2.2559
1.1010	.0000	.0358	1.6272	-.0648	.3395	2.2590
1.1185	.0000	.0364	1.6266	-.0637	.3380	2.2623
1.1359	.0000	.0370	1.6260	-.0625	.3363	2.2658
1.1634	.0000	.0377	1.6253	-.0612	.3346	2.2695
1.1708	.0000	.0384	1.6247	-.0599	.3327	2.2734
1.1883	.0000	.0391	1.6239	-.0585	.3308	2.2776
1.2057	.0000	.0399	1.6232	-.0570	.3287	2.2820
1.2232	.0000	.0407	1.6224	-.0555	.3265	2.2867
1.2406	.0000	.0415	1.6216	-.0538	.3242	2.2916
1.2581	.0000	.0424	1.6207	-.0521	.3218	2.2968
1.2755	.0000	.0433	1.6198	-.0504	.3193	2.3116
1.2930	.0000	.0442	1.6186	-.0485	.3167	2.3170
1.3104	.0000	.0452	1.6176	-.0465	.3142	2.3222
1.3279	.0000	.0462	1.6165	-.0444	.3116	2.3275
1.3453	.0000	.0473	1.6155	-.0422	.3089	2.3328
1.3628	.0000	.0484	1.6144	-.0399	.3062	2.3383
1.3803	.0000	.0496	1.6133	-.0375	.3032	2.3443
1.3977	.0000	.0508	1.6122	-.0350	.2999	2.3223
1.4152	.0000	.0521	1.6110	-.0323	.2962	2.3581
1.4326	.0000	.0535	1.6098	-.0294	.2924	2.3641
1.4501	.0000	.0549	1.6085	-.0264	.2883	2.3707
1.4675	.0000	.0565	1.6072	-.0232	.2841	2.3773
1.4850	.0000	.0581	1.6057	-.0199	.2798	2.3843
1.5024	.0000	.0597	1.6043	-.0163	.2755	2.3948
1.5199	.0000	.0615	1.6028	-.0125	.2711	2.4057
1.5373	.0000	.0634	1.6011	-.0084	.2665	2.4168
1.5548	.0000	.0654	1.5993	-.0041	.2615	2.4293
1.5722	.0000	.0675	1.5972	.0004	.2554	2.4451
1.5897	.0000	.0698	1.5950	.0052	.2490	2.4604
1.6071	.0000	.0722	1.5927	.0105	.2420	2.4768
1.6246	.0000	.0747	1.5901	.0160	.2346	2.4949
1.6421	.0000	.0774	1.5873	.0220	.2244	2.5299
1.6595	.0000	.0802	1.5844	.0284	.2133	2.5736
1.6770	.0000	.0832	1.5814	.0353	.2011	2.6105
1.6944	.0000	.0864	1.5784	.0426	.1895	2.6449
1.7119	.0000	.0898	1.5752	.0505	.1787	2.6652
1.7293	.0000	.0935	1.5716	.0590	.1670	2.7090
1.7468	.0000	.0974	1.5678	.0682	.1539	2.7538
1.7642	.0000	.1017	1.5635	.0782	.1390	2.7944
1.7817	.0000	.1062	1.5590	.0890	.1214	2.8703
1.7991	.0000	.1112	1.5539	.1007	.0992	2.9622
1.8166	.0000	.1165	1.6585	.1134	.0758	3.0680
1.8340	.0000	.1224	1.5424	.1274	.0449	3.2273

Table 4. Computed results for the Rheinboldt suction distribution problem showing the method breakdown.

ϕ	v_s^*	t^*	H_ϵ	m	ℓ	H
1.3977	.0000	.0508	1.6122	-.0349	.2997	2.3228
1.3995	.0000	.0509	1.6120	-.0347	.2994	2.3238
1.4013	.0000	.0510	1.6119	-.0344	.2990	2.3249
1.4031	.0000	.0512	1.6118	-.0341	.2986	2.3260
1.4049	.0000	.0513	1.6116	-.0339	.2983	2.3270
1.4067	.0000	.0514	1.6115	-.0336	.2979	2.3281
1.4085	.0000	.0516	1.6114	-.0333	.2975	2.3292
1.4103	.0000	.0517	1.6112	-.0330	.2971	2.3567
1.4121	.0000	.0519	1.6111	-.0328	.2968	2.3573
1.4295	.0000	.0532	1.6100	-.0299	.2930	2.3632
1.4470	.0000	.0546	1.6087	-.0270	.2890	2.3697
1.4644	.0000	.0561	1.6074	-.0238	.2848	2.3763
1.4819	.0000	.0577	1.6059	-.0205	.2805	2.3831
1.4993	.0000	.0594	1.6043	-.0169	.2760	2.3939
1.5168	1.0504	.0612	1.6029	-.0971	.3230	2.3474
1.5221	1.0665	.0612	1.6041	-.0977	.3253	2.3412
1.5275	1.0826	.0612	1.6053	-.0983	.3275	2.3353
1.5328	1.0986	.0612	1.6064	-.0989	.3296	2.3297
1.5382	1.1147	.0613	1.6074	-.0995	.3317	2.3242
1.5436	1.1308	.0613	1.6085	-.1001	.3337	2.3186
1.5489	1.1469	.0614	1.6094	-.1007	.3355	2.3139
1.5543	1.1630	.0615	1.6103	-.1013	.3371	2.3097
1.5596	1.1790	.0616	1.6111	-.1018	.3385	2.3061
1.5650	1.1951	.0617	1.6119	-.1023	.3398	2.3027
1.5704	1.2112	.0618	1.6127	-.1028	.3411	2.2988
1.5757	1.2273	.0619	1.6135	-.1033	.3425	2.2947
1.5811	1.2434	.0620	1.6142	-.1039	.3438	2.2908
1.5985	1.2957	.0624	1.6166	-.1057	.3480	2.2783
1.6160	1.3481	.0628	1.6187	-.1075	.3518	2.2672
1.6334	1.4004	.0634	1.6206	-.1094	.3553	2.2573
1.6509	1.4528	.0640	1.6222	-.1113	.3585	2.2484
1.6684	1.5052	.0647	1.6235	-.1131	.3614	2.2480
1.6858	1.5575	.0654	1.6248	-.1150	.3641	2.2430
1.7033	1.6099	.0663	1.6259	-.1169	.3665	2.2386
1.7207	1.6622	.0671	1.6268	-.1187	.3688	2.2346
1.7382	1.7146	.0681	1.6276	-.1205	.3708	2.2312
1.7556	1.7670	.0691	1.6283	-.1223	.3727	2.2282
1.7731	1.8193	.0702	1.6289	-.1240	.3743	2.2256
1.7905	1.8717	.0714	1.6293	-.1257	.3758	2.2234
1.8080	1.9240	.0726	1.6297	-.1273	.3771	2.2216
1.8254	1.9764	.0739	1.6299	-.1287	.3782	2.2202
1.8429	2.0288	.0753	1.6301	-.1301	.3792	2.2190
1.8603	2.0811	.0768	1.6301	-.1314	.3799	2.2183
1.8778	2.1335	.0784	1.6301	-.1325	.3804	2.2173
1.8952	2.1858	.0801	1.6300	-.1333	.3807	2.2175

Table 4. (Continued)

ϕ	v_s*	t*	H_ϵ	m	ℓ	H
1.9127	2.2510	.0819	1.6297	-.1361	.3818	2.2167
1.9302	2.3208	.0837	1.6294	-.1395	.3832	2.2157
1.9476	2.3906	.0857	1.6291	-.1429	.3845	2.2148
1.9651	2.4604	.0877	1.6288	-.1463	.3857	2.2141
1.9825	2.5302	.0898	1.6283	-.1496	.3869	2.2137
2.0000	2.6000	.0920	1.6278	-.1527	.3878	2.2136
2.0174	2.6698	.0944	1.6273	-.1557	.3887	2.2139
2.0349	2.7396	.0969	1.6266	-.1584	.3892	2.2146
2.0523	2.8095	.0995	1.6259	-.1609	.3896	2.2159
2.0698	2.8793	.1022	1.6251	-.1629	.3895	2.2179
2.0872	2.9491	.1052	1.6242	-.1643	.3890	2.2207
2.1047	3.0189	.1083	1.6231	-.1651	.3881	2.2242
2.1221	3.0887	.1116	1.6220	-.1649	.3865	2.2288
2.1396	3.1585	.1151	1.6207	-.1638	.3843	2.2344
2.1570	3.2283	.1189	1.6192	-.1608	.3809	2.2419
2.1745	3.2982	.1229	1.6177	-.1555	.3759	2.2487
2.1920	3.3680	.1272	1.6159	-.1475	.3693	2.2586
2.2094	3.4378	.1318	1.6140	-.1357	.3606	2.2706
2.2269	3.5076	.1368	1.6119	-.1188	.3489	2.2911
2.2443	3.5774	.1421	1.6096	-.0891	.3290	2.3197
IMPROPER SLOPES						
IMPROPER SLOPES						
IMPROPER SLOPES						
IMPROPER SLOPES						
IMPROPER SLOPES						
IMPROPER SLOPES						
IMPROPER SLOPES						
IMPROPER SLOPES						
IMPROPER SLOPES						
EXCESSIVE LOOPS						

Table 5. Computed results for the Ando suction distribution problem for ϕ = 180 degrees.

ϕ	v_s^*	t^*	H_ϵ	m	ℓ	H
1.4675	.0000	.0565	1.6072	-.0233	.2841	2.3773
1.4693	.0000	.0566	1.6070	-.0229	.2837	2.3780
1.4711	.0000	.0568	1.6068	-.0226	.2832	2.3788
1.4729	.0000	.0569	1.6067	-.0222	.2828	2.3795
1.4747	.0000	.0571	1.6065	-.0219	.2823	2.3802
1.4765	.0000	.0573	1.6064	-.0215	.2819	2.3809
1.4783	.0000	.0575	1.6062	-.0212	.2814	2.3816
1.4801	.0000	.0576	1.6061	-.0208	.2810	2.3823
1.4819	.0000	.0578	1.6059	-.0205	.2805	2.3831
1.4837	.0000	.0580	1.6057	-.0201	.2800	2.3838
1.4855	.0000	.0581	1.6056	-.0198	.2796	2.3849
1.5029	.0000	.0598	1.6042	-.0162	.2753	2.3953
1.5204	.0000	.0616	1.6027	-.0124	.2709	2.4062
1.5378	.0000	.0635	1.6010	-.0083	.2664	2.4173
1.5553	.0000	.0655	1.5992	-.0040	.2613	2.4299
1.5727	.1516	.0676	1.5971	-.0097	.2617	2.4354
1.5902	.2442	.0696	1.5959	-.0113	.2607	2.4408
1.6076	.3343	.0715	1.5948	-.0127	.2599	2.4327
1.6251	.4222	.0734	1.5937	-.0136	.2588	2.4394
1.6425	.5082	.0753	1.5929	-.0143	.2579	2.4447
1.6600	.5925	.0772	1.5922	-.0148	.2571	2.4491
1.6774	.6754	.0790	1.5916	-.0150	.2563	2.4529
1.6949	.7573	.0809	1.5912	-.0149	.2556	2.4563
1.7123	.8383	.0829	1.5907	-.0147	.2547	2.4595
1.7298	.9188	.0848	1.5904	-.0141	.2538	2.4627
1.7472	.9990	.0868	1.5900	-.0134	.2428	2.4660
1.7647	1.0793	.0889	1.5896	-.0123	.2514	2.4701
1.7822	1.1598	.0910	1.5893	-.0110	.2499	2.4747
1.7996	1.2410	.0931	1.5889	-.0094	.2481	2.4797
1.8171	1.3231	.0954	1.5885	-.0075	.2462	2.4852
1.8345	1.4063	.0977	1.5881	-.0053	.2439	2.4914
1.8520	1.4909	.1000	1.5877	-.0027	.2413	2.4984
1.8694	1.5773	.1025	1.5872	.0003	.2383	2.5070
1.8869	1.6657	.1050	1.5867	.0038	.2348	2.5162
1.9043	1.7564	.1076	1.5862	.0079	.2309	2.5264
1.9218	1.8504	.1103	1.5857	.0125	.2265	2.6377
1.9392	1.9534	.1131	1.5852	.0170	.2221	2.5493
1.9567	2.0589	.1160	1.5847	.0224	.2170	2.5678
1.9741	2.1668	.1189	1.5841	.0290	.2110	2.5818
1.9915	2.2770	.1219	1.5837	.0369	.2040	2.5941
1.9968	2.3114	.1229	1.5836	.0397	.2017	2.5987
2.0022	2.3461	.1238	1.5834	.0426	.1992	2.6059
2.0075	2.3809	.1248	1.5833	.0457	.1966	2.6106
2.0129	2.4159	.1258	1.5832	.0491	.1939	2.6155
2.0182	2.4511	.1267	1.5832	.0527	.1910	2.6206
2.0236	2.4866	.1277	1.5831	.0565	.1879	2.6258

Table 5. (Continued)

ϕ	v_s^*	t^*	H_ϵ	m	ℓ	H
2.0411	2.6032	.1310	1.5829	.0750	.1724	2.6588
IMPROPER SLOPES						
IMPROPER SLOPES						
IMPROPER SLOPES						
IMPROPER SLOPES						
IMPROPER SLOPES						
IMPROPER SLOPES						
IMPROPER SLOPES						
IMPROPER SLOPES						
IMPROPER SLOPES						
EXCESSIVE LOOPS						

Table 6. Computed results for the Ando suction distribution problem for ϕ = 270 degrees.

ϕ	v_s^*	t^*	H_ϵ	m	ℓ	H
1.4675	.0000	.0565	1.6072	-.0233	.2841	2.3773
1.4693	.0000	.0565	1.6071	-.0229	.2838	2.3778
1.4711	.0000	.0566	1.6070	-.0225	.2834	2.3783
1.4729	.0000	.0567	1.6069	-.0221	.2830	2.3788
1.4747	.0000	.0568	1.6068	-.0218	.2826	2.3793
1.4765	.0000	.0569	1.6068	-.0214	.2823	2.3798
1.4783	.0000	.0570	1.6067	-.0210	.2819	2.3802
1.4801	.0000	.0570	1.6066	-.0206	.2815	2.3807
1.4819	.0000	.0571	1.6065	-.0203	.2811	2.3812
1.4837	.0000	.0572	1.6064	-.0199	.2807	2.3817
1.5011	.0000	.0581	1.6056	-.0161	.2770	2.3895
1.5186	.0000	.0590	1.6047	-.0123	.2733	2.3979
1.5360	.0000	.0599	1.6038	-.0083	.2694	2.4067
1.5535	.0000	.0609	1.6027	-.0042	.2654	2.4156
1.5709	.1285	.0620	1.6015	-.0085	.2669	2.4154
1.5884	.1840	.0630	1.6005	-.0078	.2654	2.4198
1.6058	.2409	.0641	1.5996	-.0071	.2638	2.4248
1.6233	.2990	.0651	1.5986	-.0063	.2618	2.4306
1.6407	.3584	.0662	1.5977	-.0054	.2599	2.4195
1.6582	.4190	.0673	1.5967	-.0044	.2576	2.4280
1.6756	.4808	.0684	1.5956	-.0034	.2554	2.4362
1.6931	.5438	.0695	1.5947	-.0023	.2532	2.4442
1.7105	.6079	.0707	1.5937	-.0011	.2509	2.4520
1.7280	.6732	.0718	1.5928	.0001	.2487	2.4691
1.7454	.7396	.0730	1.5920	.0014	.2466	2.4744
1.7629	.8071	.0742	1.5912	.0029	.2444	2.4797
1.7804	.8757	.0754	1.5904	.0045	.2422	2.4851
1.7978	.9453	.0767	1.5896	.0063	.2397	2.4895
1.8153	1.0160	.0780	1.5888	.0083	.2366	2.4998
1.8327	1.0877	.0793	1.5880	.0106	.2334	2.5102
1.8502	1.1604	.0806	1.5872	.0131	.2300	2.5209
1.8676	1.2341	.0819	1.5865	.0159	.2264	2.5319
1.8851	1.3087	.0833	1.5858	.0189	.2226	2.5434
1.9025	1.3842	.0847	1.5850	.0223	.2186	2.5615
1.9200	1.4606	.0861	1.5843	.0260	.2141	2.5737
1.9374	1.5378	.0875	1.5835	.0302	.2094	2.5864
1.9548	1.6158	.0890	1.5828	.0349	.2042	2.5973
1.9722	1.6947	.0905	1.5821	.0401	.1987	2.6127
1.9896	1.7744	.0921	1.5814	.0461	.1925	2.6265
2.0070	1.8549	.0936	1.5807	.0528	.1858	2.6412
2.0244	1.9361	.0952	1.5801	.0604	.1784	2.6431
2.0418	2.0181	.0969	1.5795	.0682	.1713	2.6761
2.0592	2.1008	.0986	1.5788	.0774	.1631	2.6961
2.0766	2.1841	.1003	1.5782	.0880	.1537	2.7126
2.0940	2.2680	.1020	1.5776	.1034	.1388	2.7464

Table 6 (Continued)

ϕ	v_s*	t*	$H\epsilon$	m	ℓ	H
IMPROPER SLOPES						
IMPROPER SLOPES						
IMPROPER SLOPES						
IMPROPER SLOPES						
IMPROPER SLOPES						
IMPROPER SLOPES						
IMPROPER SLOPES						
IMPROPER SLOPES						
IMPROPER SLOPES						
EXCESSIVE LOOPS						

Table 7. Computed results for a uniform porosity cylinder suction distribution showing the off chart difficulty $A = 65$, $B = 16$, $\phi_s = 270$ degrees

$v_s^* = \sqrt{A - B\,(\sin\phi - \sin\phi_s)^2}$

ϕ	v_s^*	t^*	H_ϵ	m	ℓ	H
1.4675	.0000	.0565	1.6072	-.0233	.2841	2.3773
1.4693	.0000	.0565	1.6071	-.0229	.2838	2.3778
1.4711	.0000	.0566	1.6070	-.0225	.2834	2.3783
1.4729	.0000	.0567	1.6069	-.0221	.2830	2.3788
1.4747	.0000	.0568	1.6068	-.0218	.2826	2.3793
1.4765	.0000	.0569	1.6068	-.0214	.2823	2.3798
1.4783	.0000	.0570	1.6067	-.0210	.2819	2.3802
1.4801	.0000	.0570	1.6066	-.0206	.2815	2.3807
1.4819	.0000	.0571	1.6065	-.0203	.2811	2.3812
1.4837	.0000	.0572	1.6064	-.0199	.2807	2.3817
1.4855	.0000	.0573	1.6063	-.0195	.2803	2.3822
1.4873	.0000	.0574	1.6062	-.0191	.2800	2.3827
1.5047	.0000	.0582	1.6054	-.0153	.2762	2.3913
1.5222	.0000	.0592	1.6045	-.0115	.2724	2.3998
1.5396	.0000	.0601	1.6035	-.0074	.2685	2.4086
1.5571	.0000	.0611	1.6024	-.0033	.2645	2.4176
1.5745	1.0002	.0622	1.6012	-.0760	.3082	2.3562
1.5920	1.0071	.0625	1.6026	-.0724	.3084	2.3474
1.6094	1.0236	.0629	1.6038	-.0695	.3088	2.3401
1.6269	1.0491	.0633	1.6048	-.0674	.3091	2.3341
1.6443	1.0830	.0637	1.6057	-.0659	.3096	2.3454
1.6618	1.1246	.0643	1.6063	-.0650	.3100	2.3438
1.6792	1.1729	.0648	1.6068	-.0647	.3106	2.3421
1.6967	1.2271	.0654	1.6072	-.0648	.3114	2.3403
1.7141	1.2865	.0660	1.6076	-.0655	.3123	2.3383
1.7316	1.3503	.0666	1.6079	-.0665	.3134	2.3362
1.7490	1.4179	.0673	1.6082	-.0680	.3147	2.3131
1.7665	1.4887	.0680	1.6086	-.0700	.3165	2.3099
1.7840	1.5623	.0687	1.6089	-.0722	.3185	2.3070
1.8014	1.6382	.0694	1.6093	-.0748	.3205	2.3277
1.8189	1.7160	.0701	1.6094	-.0776	.3223	2.3257
1.8363	1.7955	.0708	1.6096	-.0806	.3243	2.3234
1.8538	1.8764	.0716	1.6098	-.0839	.3265	2.3209
1.8712	1.9584	.0723	1.6099	-.0875	.3288	2.3182
1.8887	2.0413	.0731	1.6101	-.0914	.3313	2.3155
1.9061	2.1251	.0739	1.6103	-.0956	.3340	2.3126
1.9236	2.2095	.0747	1.6106	-.1002	.3369	2.3090
1.9410	2.2943	.0755	1.6107	-.1049	.3398	2.3060
1.9585	2.3796	.0763	1.6109	-.1099	.3428	2.3017
1.9759	2.4652	.0771	1.6112	-.1152	.3460	2.2970
1.9934	2.5510	.0779	1.6114	-.1209	.3493	2.2921
2.0108	2.6369	.0788	1.6118	-.1270	.3530	2.2868
2.0283	2.7228	.0797	1.6121	-.1334	.3568	2.2892
2.0458	2.8088	.0805	1.6124	-.1402	.3608	2.2755

Table 7. (Continued)

ϕ	v_s*	t*	H_ϵ	m	ℓ	H
2.0632	2.8946	.0814	1.6127	-.1475	.3650	2.2715
2.0807	2.9804	.0824	1.6130	-.1550	.3693	2.2679
2.0981	3.0659	.0833	1.6134	-.1628	.3735	2.2646
2.1156	3.1512	.0842	1.6137	-.1711	.3780	2.2518
2.1330	3.2363	.0852	1.6140	-.1798	.3826	2.2549
2.1505	3.3211	.0862	1.6142	-.1888	.3873	2.2514
2.1679	3.4055	.0872	1.6144	-.1981	.3921	2.2480
2.1854	3.4895	.0883	1.6145	-.2076	.3966	2.2388
2.2028	3.5732	.0894	1.6147	-.2177	.4015	2.2410
2.2203	3.6564	.0905	1.6147	-.2274	.4057	2.2372
2.2377	3.7391	.0916	1.6147	-.2371	.4098	2.2297
2.2552	3.8214	.0928	1.6147	-.2475	.4142	2.2270
2.2726	3.9031	.0939	1.6147	-.2576	.4181	2.2254
2.2901	3.9843	.0952	1.6146	-.2678	.4219	2.2248
2.3076	4.0649	.0964	1.6144	-.2771	.4249	2.2245
2.3250	4.1450	.0977	1.6142	-.2867	.4278	2.2243
2.3425	4.2244	.0990	1.6140	-.2966	.4309	2.2241
2.3599	4.3032	.1004	1.6137	-.3058	.4333	2.2266
2.3774	4.3814	.1018	1.6134	-.3147	.4354	2.2312
2.3948	4.4589	.1033	1.6130	-.3233	.4372	2.2361
2.4123	4.5358	.1048	1.6125	-.3318	.4388	2.2416
2.4297	4.6119	.1063	1.6118	-.3400	.4402	2.2432
2.4472	4.6874	.1079	1.6112	-.3481	.4415	2.2449
2.4646	4.7621	.1096	1.6105	-.3562	.4427	2.2468
2.4821	4.8361	.1113	1.6097	-.3639	.4436	2.2492
2.4995	4.9093	.1130	1.6089	-.3714	.4444	2.2520
2.5170	4.9817	.1149	1.6080	-.3788	.4451	2.2589
2.5344	5.0534	.1168	1.6070	-.3853	.4453	2.2663
2.5519	5.1243	.1187	1.6059	-.3908	.4449	2.2741
2.5694	5.1943	.1208	1.6046	-.3938	.4431	2.2830
OFF CHART						

APPENDIX G

Additional Figures

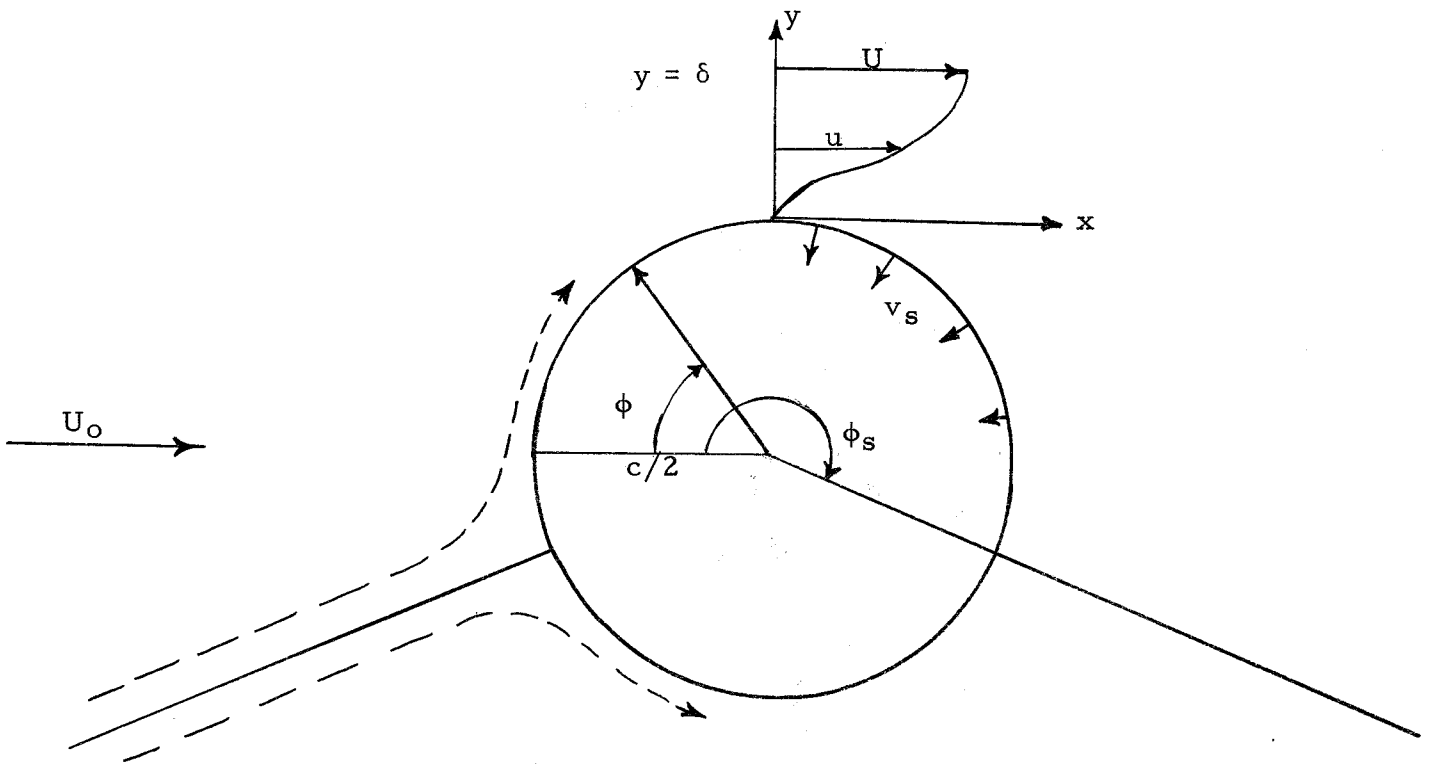

Figure 20. Geometry of the circular cylinder with the coordinates used.

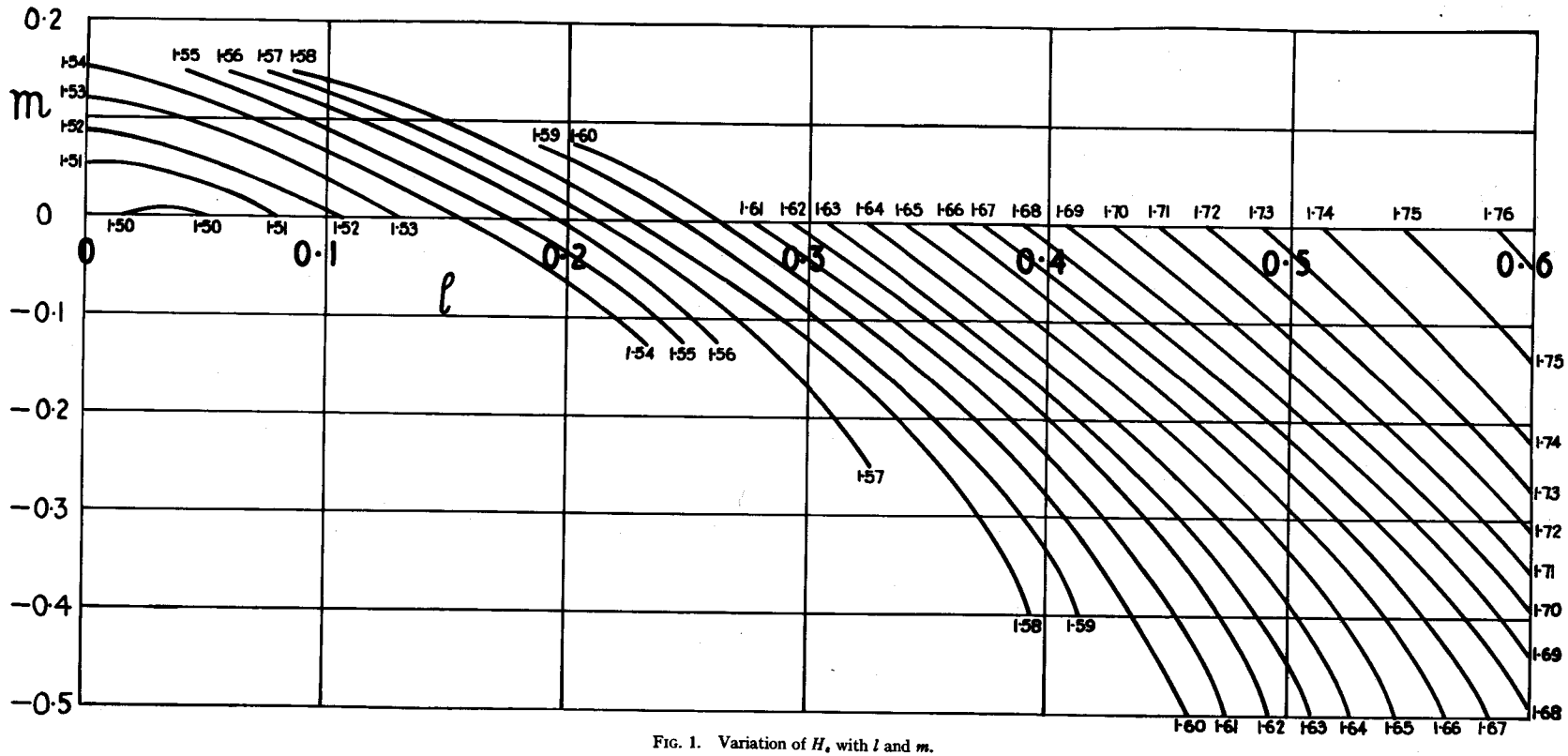

FIG. 1. Variation of H_s with l and m.

Figure 21. Reproduction of Figure 1 of Head's paper (4, p. 26)

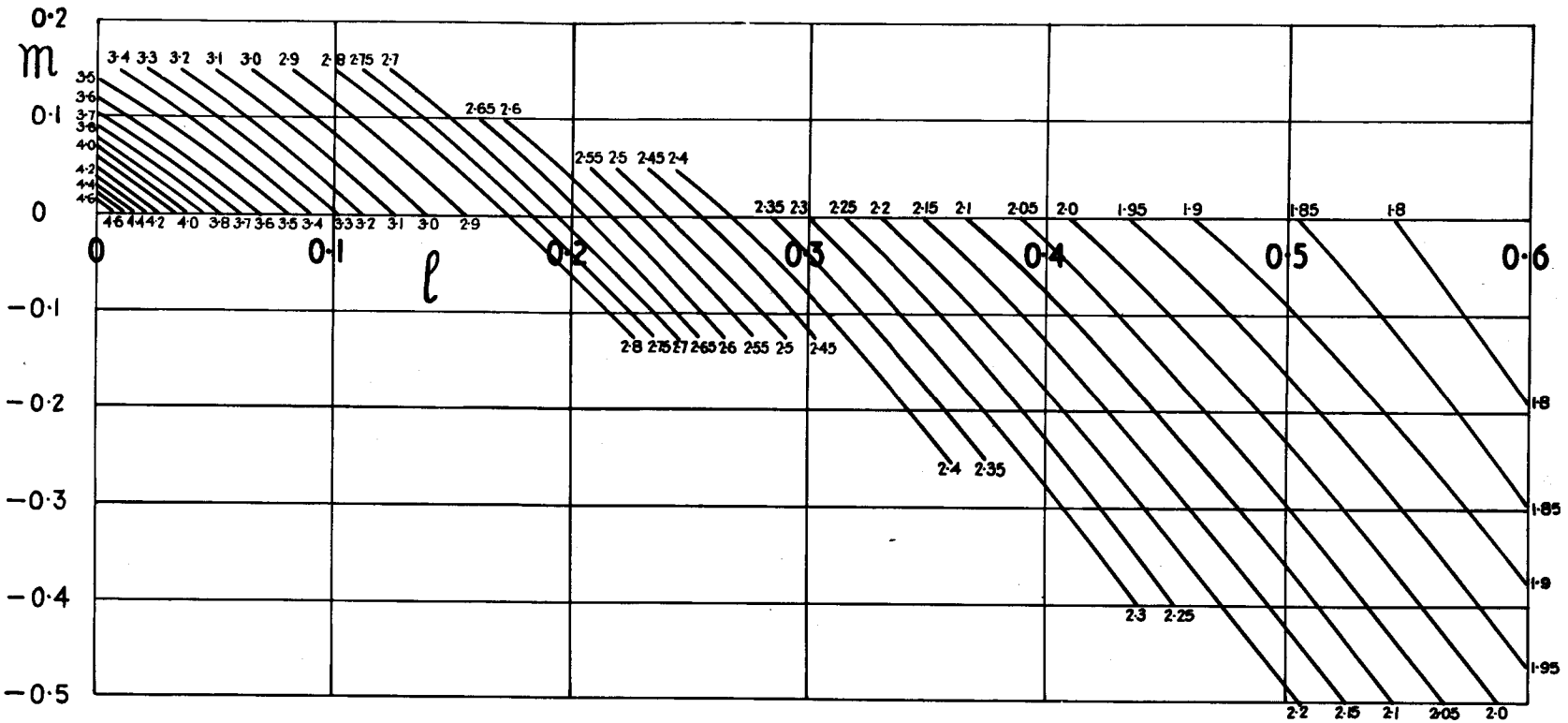

FIG. 2. Variation of H with l and m.

Figure 22. Reproduction of Figure 2 of Head's paper (4, p. 26)

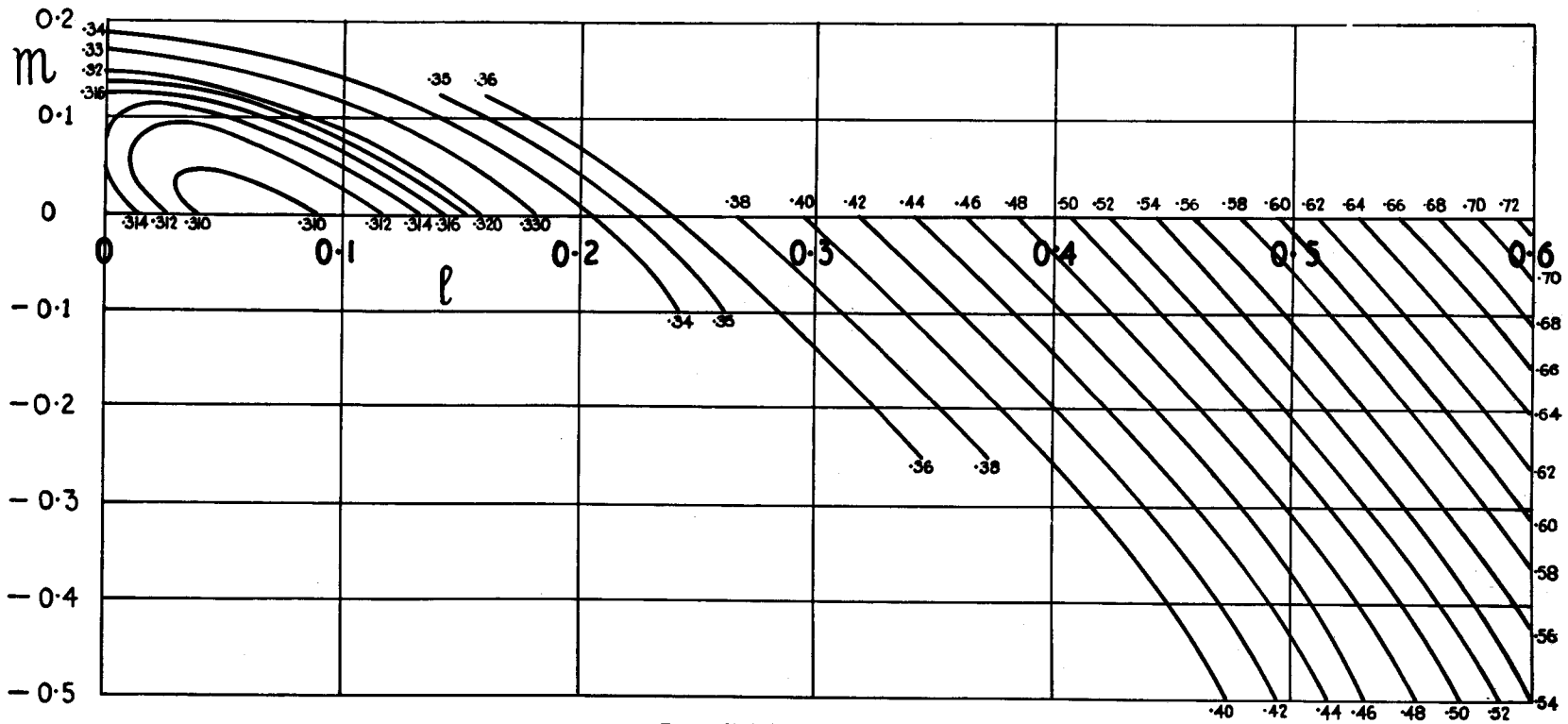

FIG. 3. Variation of $2D^*$ with l and m.

Figure 23. Reproduction of Figure 3 of Head's paper (4, p. 26)

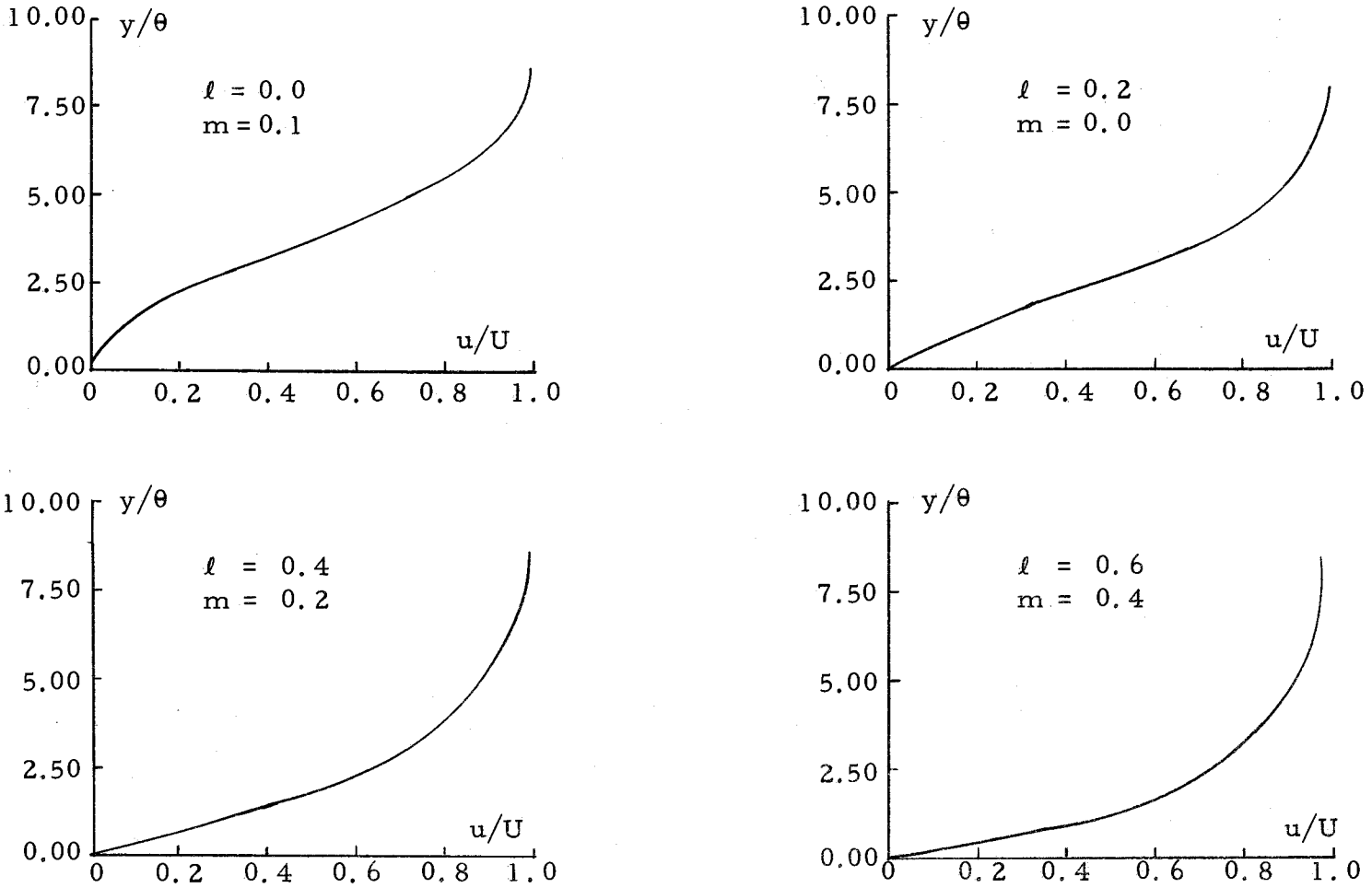

Figure 24. Four typical profiles for different combinations of ℓ and m.